

# Anomalous geometric transport signatures of topological Euler class

Ashwat Jain,<sup>1,\*</sup> Wojciech J. Jankowski,<sup>2,†</sup> and Robert-Jan Slager<sup>3,2,‡</sup>

<sup>1</sup>*Mathematical Institute, University of Oxford, Andrew Wiles Building, Woodstock Road, Oxford, OX2 6GG, UK*

<sup>2</sup>*Theory of Condensed Matter Group, Cavendish Laboratory, University of Cambridge, J. J. Thomson Avenue, Cambridge CB3 0HE, UK*

<sup>3</sup>*Department of Physics and Astronomy, University of Manchester, Oxford Road, Manchester M13 9PL, UK*

(Dated: December 3, 2024)

We investigate Riemannian quantum-geometric structures in semiclassical transport features of two-dimensional multigap topological phases. In particular, we study nonlinear Hall-like bulk electric current responses and, accordingly, semiclassical equations of motion induced by the presence of a topological Euler invariant. We provide analytic understanding of these quantities by phrasing them in terms of momentum-space geodesics and geodesic deviation equations and further corroborate these insights with numerical solutions. Within this framework, we moreover uncover anomalous bulk dynamics associated with the second- and third-order nonlinear Hall conductivities induced by a patch Euler invariant. As a main finding, our results show how one can reconstruct the Euler invariant on coupling to electric fields at nonlinear order and from the gradients of the electric fields. Furthermore, we comment on the possibility of deducing the non-trivial non-Abelian Euler class invariant specifically in second-order nonlinear ballistic conductance measurements within a triple-contact setup, which was recently proposed to probe the Euler characteristics of more general Fermi surfaces. Generally, our results provide a route for deducing the topology in real materials that exhibit the Euler invariant by analyzing bulk electrical currents.

*Introduction.*— Anomalous electrodynamic responses constitute a key experimental signature of topological phases of matter [1–3]. These responses are related to field-theoretic anomalies realized in topological vacua. In two spatial dimensions, quantum Hall effects, for example, are manifested by transverse dissipationless currents. Consequently, the appearance of this effect in the context of Chern insulators can be understood as a consequence of the parity anomaly [4, 5], as further supported by the Chern-Simons theories. In three dimensions, topological  $\mathbb{Z}_2$  insulators and axion insulators, recently shown to exist in manganese-doped bismuth telluride compounds [6, 7], can realize topological  $\theta$ -terms [8, 9], which in turn lead to an anomalous topological magnetoelectric effect. Similarly, Weyl semimetals are associated with chiral anomalies [10–12], and are understood in terms of the dynamics of axial gauge fields emergent from non-trivial band topology [13]. Moreover, apart from these electromagnetic anomalies, topological matter has been shown to exhibit an interplay with background geometry, as realized through gravitational-axial anomalies in Weyl semimetals [14, 15], or non-trivial torsional responses [16–21]. Gravitational anomalies in topological materials [22] open new avenues for exotic phenomena associated with Hall viscosity and elastic responses [23].

The aforementioned anomalies are by and large associated with single gap and gapless topologies, which are extensively classified [24–29]. In contrast, the anomalous electrodynamic responses of more recently intro-

duced systems with multiple topological band gaps [30–33] that require finite band partitionings to culminate in multiband invariants classified via homotopy theory, remain rather unexplored, although the first quantized optical responses therein were recently identified [34, 35]. A paradigmatic multigap topological invariant is the Euler class [30, 36–38] protected by  $\mathcal{C}_2\mathcal{T}$  (i.e. two-fold rotation combined with time-reversal) symmetry, which can be associated with the non-Abelian nodal charges and their braiding processes between different gaps. That is, due to the anticommutative nature of band node charges in such systems [39], braiding them in momentum space can result in a set of two bands with similarly, rather than oppositely, charged nodes. Similar charges prevent the nodes from annihilating, which is encapsulated by a nonzero Euler class that can only alter upon braiding with a node in an adjacent band gap [37, 38].

The absence of an anomalous transport signature of Euler topology is an open problem, which we address in this work. The Euler invariant  $\chi \in \mathbb{Z}$  defined for a pair of adjacent bands  $|u_n\rangle, |u_{n+1}\rangle$  reads [30, 36–38]

$$\chi = \frac{1}{2\pi} \int_{\mathcal{D}} \text{Eu} - \frac{1}{2\pi} \int_{\partial\mathcal{D}} a, \quad (1)$$

with the Euler curvature  $\text{Eu} = da$  defined from the non-Abelian Euler connection  $a = \langle u_n | du_{n+1} \rangle$  over a Brillouin zone (BZ) patch  $\mathcal{D} \in \text{BZ}$  [38]. Although the non-Abelian Euler topologies are established in quantum simulators [40–42], through metamaterial realizations [43, 44], phonon bands [45, 46], in out-of-equilibrium phases [40, 47], are predicted in real material/magnetic [38, 48, 49], and more recently, interacting [50] contexts; these phases appear elusive to dc transport signatures. In particular, under  $\mathcal{C}_2\mathcal{T}$  symmetry, the Berry curvature in the occupied bands vanishes identically. Hence, the standard

\* ashwat.jain@wadham.ox.ac.uk; Contributed equally.

† wjj25@cam.ac.uk; Contributed equally.

‡ rjs269@cam.ac.uk;

anomalous Hall velocity of electrons vanishes in Euler phases, whereas the entire topology-induced geometric transport can be captured by a quantum metric, which is real and positive-semidefinite [51–54]. In particular, any band node associated with the Euler invariant can be viewed as a quantum-metric singularity. Such a singularity can in some context be thought of as a momentum-space black hole, in a sense that its momentum-space Kretschmann invariant [55], i.e. a scalar constructed from the contraction of the Riemann curvature tensor with itself, diverges at the band node; see Fig. 1.

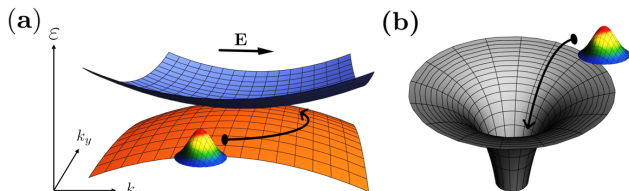


**FIG. 1.** (a) Non-Abelian band singularity hosting a non-trivial patch Euler class  $\chi$  and realizing anomalous wavepacket dynamics. (b) Associated momentum-space quantum metric singularity due to topologically non-trivial Euler node. The Riemannian geometry is fingerprinted through the momentum-space Christoffel symbols and Riemann curvature tensor associated with the singularity in the quantum metric induces anomalous wavepacket dynamics and nonlinear bulk current responses allowing a reconstruction of the Euler invariant.

The Euler invariant can be viewed as a winding of an interband dipole moment; in direct contrast to the winding of the ground-state electric polarization that defines the well-established Chern invariant. As a consequence, the optical effects in response to the ac electric fields can be quantized. Correspondingly, it was shown that the Euler invariant can induce a quantized optical conductivity and the ratios of third-order jerk photoconductivities [56] quantized by the invariant [34], on leveraging the associated singular quantum-geometric conditions [54]. Given the interplay of ac and dc responses, as underpinned by the Kramers-Kronig relations, this provides further possibilities that the multiband invariant can be extracted from the responses to static electric fields [34], especially as the multiband contributions are known to emerge in the field-induced corrections of the nonlinear transport [57].

In this work, we study anomalous transport signatures associated with the quantum geometry of the non-Abelian bands hosting a multigap Euler topology. We show that, despite the vanishing Hall responses at linear order, there are enhanced nonlinear geometric responses in dc transport present, which we retrieve from the equations of motion of individual wavepackets. While in centrosymmetric Euler phases, the combined second-order bulk responses need to vanish by the inversion symmetry, the non-centrosymmetric Euler bands realize the second-order quantum-metric nonlinear Hall effect [58]

and responses to electric-field gradients induced by the quantum-metric dipole [59]. Finally, and most importantly, we show that the Euler bands universally provide for a third-order Hall response [60–64] in the non-degenerate limit, and hence that Euler bands can realize higher-order dissipationless currents. As a consequence, we showcase bulk observable anomalous dc transport signatures of nodal Euler band topology.

*Multiband Riemannian quantum geometry.*— To retrieve the multiband quantum-geometric electric transport responses induced by the Euler invariant, we define the momentum-space geometric background induced by the topological bands. We begin with the definition of the multiband quantum metric [34, 51–54] realized by bands  $n, m$

$$g_{\alpha\beta}^{mn} = \frac{1}{2} \left[ \langle \partial_{k_\alpha} u_{n\mathbf{k}} | u_{m\mathbf{k}} \rangle \langle u_{m\mathbf{k}} | \partial_{k_\beta} u_{n\mathbf{k}} \rangle + \text{c.c.} \right], \quad (2)$$

which is manifestly real and symmetric, and defines a quantum distance  $ds_{mn}^2 = g_{\alpha\beta}^{mn} dk_\alpha dk_\beta$ , where we assumed Einstein summation convention, as in the rest of this work. Furthermore, we define a combined band-weighted quantum metric as

$$\mathcal{G}_{\alpha\beta}^n = \sum_{\{m\}} c_{mn} g_{\alpha\beta}^{mn}, \quad (3)$$

where one can restrict the sum to involve all the other bands  $m \neq n$ , or otherwise, specifically the unoccupied bands (unocc) [34, 52–54]. Notably, setting  $c_{mn} = 1$  for unoccupied bands ( $m$ ) retrieves the total quantum metric in the occupied bands  $g_{\alpha\beta}^n = \sum_m^{\text{unocc}} g_{\alpha\beta}^{mn}$ .  $g_{\alpha\beta}^n$  is related to the electric quadrupole moment in the bands and hence couples to the nonuniform electric fields through its derivatives [59, 65]. On the contrary, setting the weighting coefficients to band energy weights  $c_{mn} = \hbar / (\epsilon_{n\mathbf{k}} - \epsilon_{m\mathbf{k}})$  retrieves a weighted quantum-metric  $G_{\alpha\beta}^n = \hbar \sum_{m \neq n} g_{\alpha\beta}^{mn} / (\epsilon_{n\mathbf{k}} - \epsilon_{m\mathbf{k}})$ , which through its momentum-space multipoles enters the nonlinear responses to static uniform electric fields [57]. The generalized quantum-metric similarly defines a renormalized momentum-space background geometry  $ds_n^2(\{c_{mn}\}) = \mathcal{G}_{\alpha\beta}^n dk^\alpha dk^\beta$ . In this work, we utilize such weighted quantum geometries probed by both types of couplings to electric fields. In particular, a band node with non-trivial Euler invariant provides for a singularity in both considered types of weighted quantum metrics.

Furthermore, we define the Christoffel symbols for the connections in the weighted quantum metrics,

$$\Gamma_{\alpha\beta\gamma}^n = \frac{1}{2} (\partial_{k_\gamma} \mathcal{G}_{\alpha\beta}^n + \partial_{k_\beta} \mathcal{G}_{\alpha\gamma}^n - \partial_{k_\alpha} \mathcal{G}_{\beta\gamma}^n), \quad (4)$$

and the weighted Riemannian curvature tensor  $\mathcal{R}_{\alpha\beta\gamma\delta}^n = \partial_{k_\gamma} \Gamma_{\alpha\beta\delta}^n - \partial_{k_\delta} \Gamma_{\alpha\beta\gamma}^n + [\Gamma_{\alpha\delta}^n, \Gamma_{\beta\gamma}^n]$ . Additionally, under the vanishing commutation of the second term,  $[\Gamma_{\alpha\delta}^n, \Gamma_{\beta\gamma}^n] \equiv \Gamma_{\mu\alpha\delta}^n \Gamma_{\beta\mu\gamma}^n - \Gamma_{\nu\beta\gamma}^n \Gamma_{\alpha\nu\delta}^n = 0$  (see App. B), the weighted Riemannian curvature tensor reduces in

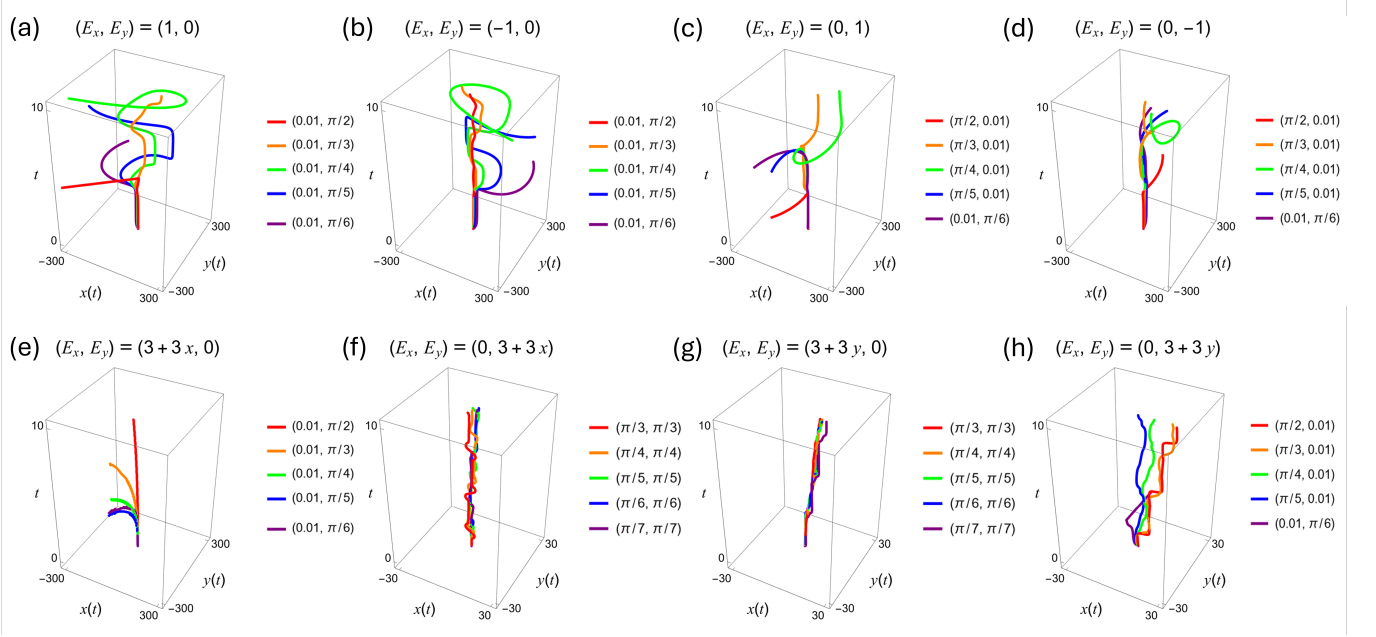


**FIG. 2.** Anomalous wavepacket dynamics induced by the singular Euler band topology. **(a-d)** Wavepacket trajectories traced by the wavepacket center of mass  $\mathbf{r}_c$  in two-dimensional real space plane  $x - y$  as a function of time  $t$  on nonlinear quadratic coupling to uniform electric field  $\alpha = E_i^2$  for different initial centre-of-mass momenta  $\mathbf{k}_c$  with different field geometries  $\mathbf{E} = (E_x, E_y)$ : **(a)**  $(1, 0)$ , **(b)**  $(-1, 0)$ , **(c)**  $(0, 1)$ , **(d)**  $(0, -1)$ . **(e-h)** Wavepacket trajectories in two-dimensional real space plane  $x - y$  as a function of time  $t$  on coupling to constant electric field gradient  $\alpha = \partial_i E_j$  for different initial centre-of-mass momenta  $\mathbf{k}_c$  for distinct electric fields  $\mathbf{E} = (E_x, E_y)$ : **(e)**  $(3 + 3x, 0)$ , **(f)**  $(0, 3 + 3x)$ , **(g)**  $(3 + 3y, 0)$ , **(h)**  $(0, 3 + 3y)$ .

terms of the quantum metric to

$$\mathcal{R}_{\alpha\beta\gamma\delta}^n = \frac{1}{2}(\partial_{k_\alpha}\partial_{k_\beta}\mathcal{G}_{\gamma\delta}^n + \partial_{k_\gamma}\partial_{k_\delta}\mathcal{G}_{\alpha\beta}^n - \partial_{k_\alpha}\partial_{k_\gamma}\mathcal{G}_{\beta\delta}^n - \partial_{k_\beta}\partial_{k_\delta}\mathcal{G}_{\alpha\gamma}^n). \quad (5)$$

These Riemannian-geometric quantities will be central objects for the wavepacket dynamics and the Euler-invariant reconstruction scheme, as well as for the bulk second- and third-order anomalous dc responses in the next and the following sections, respectively.

*Anomalous Euler wavepacket dynamics.*— We now focus on the semiclassical dynamics of the individual wavepackets realizing topologically-induced non-trivial quantum-geometry of the non-Abelian Euler bands. We construct geodesic and geodesic deviation equations for the wavepacket dynamics, which account for the previously defined Riemannian geometry of constituent Bloch states hosting a non-Abelian topology. We consider wavepackets of form [59, 66]

$$|\psi_n(t)\rangle = \int d\mathbf{k}' a(\mathbf{k}', t) e^{i\mathbf{k}' \cdot \hat{\mathbf{r}}} |\tilde{u}_{n\mathbf{k}'}\rangle, \quad (6)$$

in perturbed Bloch bands with band indices  $n$ , and with  $\hat{\mathbf{r}}$  denoting the position operator (see also App. A). More specifically, we consider the envelope functions  $|a(\mathbf{k}', t)|^2 \approx \delta(\mathbf{k}_c(t) - \mathbf{k}')$  that are sharply centred around the centre-of-mass momentum  $\mathbf{k}_c$ .

The geometric corrections induced by the non-trivial Euler class enter the wavepacket motion in addition to

the intraband dispersion term, which is fully deduced by the band energies that can be reconstructed from ARPES experiments. While the Abelian Berry curvature vanishes in Euler bands by symmetry, the perturbative field-induced correction to the Berry curvature is non-vanishing, acts as a momentum-space gauge field strength inducing a force, and cannot be neglected in the Euler bands. The field-induced Berry curvature correction  $\tilde{\Omega}_n(\mathbf{E}) = \nabla_{\mathbf{k}} \times \mathbf{A}'_{nn}(\mathbf{E})$  is given by the gauge-invariant field-induced Berry connection correction, reading componentwise,  $A'_{nn}{}^\alpha(\mathbf{E}) = G_{\alpha\beta}^n E_\beta$  [57]. At the same order, that is quadratic in electric field strength ( $E^2$ ), a band energy correction-induced weighted metric derivative emerges (see App. A), which, unlike the former term, yields vanishing net contributions by the periodicity of band energies, when the response of all particles in a band is summed. Finally, the presence of nonuniform electric fields couples to the conventional quantum metric derivatives, which define momentum-space Christoffel symbols central to the geodesic equations [67]. Upon combining, this yields an overall semiclassical equation of motion [57, 59, 66–68],

$$(\dot{\mathbf{r}}_c)_\alpha = \frac{1}{\hbar} \partial_{k_\alpha} \varepsilon_{n\mathbf{k}} - \frac{e}{\hbar} [\mathbf{E} \times \tilde{\Omega}_n(\mathbf{E})]_\alpha + \frac{e^2}{\hbar^2} \partial_\alpha \mathcal{G}_{\beta\gamma}^n (E^2) E_\beta E_\gamma + \frac{e}{2\hbar} \partial_\alpha \mathcal{G}_{\beta\gamma}^n (\nabla) \partial_\beta E_\gamma. \quad (7)$$

Here, we implicitly assumed the well-known coupled semiclassical equation of motion for the wavepacket

centre-of-mass momentum that reads

$$(\dot{\mathbf{k}}_c)_\alpha = \frac{1}{\hbar} F_\alpha(\mathbf{r}_c) = -\frac{e}{\hbar} E_\alpha(\mathbf{r}_c), \quad (8)$$

with a force  $F_\alpha(\mathbf{r}_c)$  coupling to the wavepacket centre-of-mass  $\mathbf{r}_c$ , as given by the electric field  $E_\alpha(\mathbf{r}_c)$ . In this work, we assume that the external magnetic fields are vanishing. Hence, the time-reversal symmetry,  $\mathcal{T}^2 = -1$ , is *not* explicitly broken, but can be broken spontaneously.

Furthermore, using this generalized semiclassical geodesic equation (see App. A for the derivation), we derive a geodesic deviation equation (App. B), which introduces the Riemann tensor and is retrieved in the third-order Hall response central to the next section. The momentum-space geodesic deviation equation reads

$$\partial_{k_\delta}(\dot{\mathbf{r}}_c)_\gamma - \partial_{k_\gamma}(\dot{\mathbf{r}}_c)_\delta = \mathcal{R}_{\alpha\beta\gamma\delta}^n(\dot{\mathbf{k}}_c)_\alpha(\dot{\mathbf{k}}_c)_\beta, \quad (9)$$

which explicitly captures the deflection of the velocities of wavepackets with different centre-of-mass momenta  $\dot{\mathbf{k}}_c$  induced by the momentum-space Riemann curvature  $\mathcal{R}_{\alpha\beta\gamma\delta}^n$ . Similarly, here  $(\dot{\mathbf{k}}_c)_\beta$  can be controlled with the electric field strengths  $E_\beta$ , as follows from the other semiclassical equation of motion.

In Fig. 2, we present the anomalous evolution of the Euler band wavepackets described by the geodesic equation induced in a model Euler Hamiltonian on the kagome lattice (see App. C). We solve the coupled differential equations numerically (as detailed in App. D), and retrieve the momentum-space horizons for the quantum metric (see App. E), which separate the BZ regions for centre-of-mass wavepacket momenta  $\mathbf{k}_c$  to fall, or time-evolve, into the singular quantum states at the band nodes. We further analytically support these findings using an effective  $\mathbf{k} \cdot \mathbf{p}$  model for an Euler singularity (App. F). Physically, crossing the momentum-space horizon corresponds to the singular interband transfer of the wavepackets, where the initial wavepackets were constructed in a given band  $n$ . Manifestly, the metric derivatives governing the wavepacket evolution fingerprint the non-Abelian Berry connections on asymptotic completion to a flat (constant) metric at the  $k$ -space infinity within the effective continuum model, and hence allow to completely reconstruct the patch Euler invariant (see App. G). Upon combining the responses of individual wavepackets realized in the bands, the net bulk transport responses can be obtained (see App. H). We address such anomalous responses in the next section.

*Bulk anomalous currents from non-Abelian bands.*— Further to the anomalous dynamics of individual wavepackets governed by the quantum-geometric geodesic equation, we study bulk nonlinear responses induced by the quantum geometry of the Euler phases at different voltage-controllable dopings. With  $\mathcal{C}_2\mathcal{T}$  symmetry necessary for the realization of the fermionic Euler invariant, two scenarios emerge (i) when  $(\mathcal{C}_2\mathcal{T})^2 = 1$ , with  $(\mathcal{C}_2)^2 = -1$  and  $\mathcal{T}^2 = -1$ , or (ii)  $(\mathcal{C}_2\mathcal{T})^2 = 1$ , with  $(\mathcal{C}_2)^2 \neq -1$  and  $\mathcal{T}^2 \neq -1$ , i.e. both individual

crystalline and time-reversal symmetries are implicitly broken in the free Hamiltonian. In the latter case, second-order responses constitute a dominant contribution within the anomalous transport. Under the inversion symmetry [ $\mathcal{P} \sim \mathcal{C}_2$  in two spatial dimensions], the second-order currents vanish, and the third-order Hall response becomes dominant. In the non-centrosymmetric case, the quantum-geometric second-order nonlinear current densities can emerge. For non-centrosymmetric cases, we consider same models but with inversion-symmetry-breaking perturbations of strength  $A$ , which yield a modified Hamiltonian  $H(\mathbf{k}) \rightarrow H(\mathbf{k}) + A \sin k_x 1$  (see App. C for more details). Under the nonuniform electric fields, in inversion-free systems, we evaluate geometric currents,  $j_\gamma(\nabla) = \sigma_{\gamma,\alpha\beta}(\nabla) \partial_\alpha E_\beta$ , following Ref. [59], with the corresponding dispersive conductivity tensor contributions,

$$\sigma_{\gamma,\alpha\beta}(\nabla) = -\frac{e^2}{2\hbar} \int_{\mathbf{k}} \sum_n f_{n\mathbf{k}}(\mu) \partial_\gamma \mathcal{G}_{\alpha\beta}^n(\nabla), \quad (10)$$

where  $\int_{\mathbf{k}} \equiv \int_{\text{BZ}} \frac{d^2\mathbf{k}}{(2\pi)^2}$  denotes the momentum-space integral over the BZ, and particularly in this section, we use a shortcut notation  $\partial_\alpha = \partial_{k_\alpha}$ . Here,  $f_{n\mathbf{k}}(\mu) = [\exp(\frac{\varepsilon_{n\mathbf{k}} - \mu}{T}) + 1]^{-1}$  is a filling factor given by the chemical potential ( $\mu$ ) within the equilibrium Fermi-Dirac distribution. For second order in electric field, we acquire  $j_\gamma(E^2) = \sigma_{\gamma,\alpha\beta}(E^2) E_\alpha E_\beta$ , where here we focus on the quantum-metric dipole-induced Hall response contributed by the gradients of  $\mathcal{G}_{\alpha\beta}^n(E^2)$  [57, 69],

$$\sigma_{\gamma,\alpha\beta}^H(E^2) = -\frac{e^3}{\hbar^2} \int_{\mathbf{k}} \sum_n f_{n\mathbf{k}}(\mu) \left( \partial_\gamma \mathcal{G}_{\alpha\beta}^n - \frac{1}{2} \partial_{(\alpha} \mathcal{G}_{\beta)\gamma}^n \right), \quad (11)$$

where  $(\dots)$  denotes a symmetrization with respect to the spatial indices. Effectively, one obtains such nonlinear Hall response from the BZ integration of the individual wavepacket contributions. In noncentrosymmetric Euler semimetals, such response arises from the topologically-induced net quantum-metric dipole present in the integrand, as induced by the singular Euler node geometry (see App. I).

In the other case, when the inversion and time-reversal symmetry are present, the second order responses and the responses to nonuniform electric field vanish due to the transformation of the forcing vectors and corresponding conductivities under the inversion symmetry. In that case, the dominant quantum-geometric current contribution of interest emerges from the *third-order* responses [60, 61, 63, 64]. More concretely, the quantum-geometric third-order contribution to currents,  $j_\delta(E^3) = \sigma_{\delta,\alpha\beta\gamma}(E^3) E_\alpha E_\beta E_\gamma$ , amounts to the third-order quantum-metric quadrupole-induced Hall conductivity that reads [63],

$$\sigma_{\delta,\alpha\beta\gamma}^H(E^3) = \frac{2e^4\tau}{3\hbar^3} \int_{\mathbf{k}} \sum_n f_{n\mathbf{k}}(\mu) [\partial_\alpha \partial_{(\delta} \mathcal{G}_{\beta\gamma)}^n - \partial_{(\beta} \partial_\gamma \mathcal{G}_{\delta)\alpha}^n]. \quad (12)$$

Here,  $\tau$  is a scattering time, as the third-order quantum-geometric Hall conductivity contributions in the  $\mathcal{PT}$ -symmetric systems with inversion symmetry are only extrinsic, unlike the second-order quantum-geometric Hall conductivity contributions [63]. The third-order conductivity acquires contributions from the generalized Riemann curvature tensor  $\mathcal{R}_{\alpha\beta\gamma\delta}^n$ . For more details, see App. F and App. G.

In Fig. 3, we show the results in the zero-temperature ( $T = 0$ ) limit for different chemical potentials  $\mu$  in both inversion-symmetric and inversion-symmetry-free kagome Euler Hamiltonians. We observe that changing the doping allows one to explicitly infer the geometry of the non-Abelian bands over BZ, which ultimately allows to deduce the Euler invariant. Finally, we retrieve the chemical potential-dependent scaling of these bulk third-order and second-order currents in the effective continuum Euler Hamiltonians in App. I, which analytically supports the numerical results in realistic lattice-regularized Hamiltonians.

*Conductance and Fermi surface topology.*— Finally, following the insights of Ref. [70], we consider nonlinear ballistic conductance signatures of the Euler phases, emerging from the Fermi surface topology, on doping away from the Euler nodes. As pointed out in the context of graphene, the presence of band nodes allows to control the Euler characteristic  $\chi_F$  of electron and hole Fermi surfaces. A single band crossing allows to introduce  $\chi_F = \text{sgn}(E_F - E_0)$  on doping away from the band node energy  $E_0$ . Furthermore, the intrinsic nonlinear conductance  $\alpha_i(\omega_1, \omega_2)$  in response to electric potential perturbations  $V_1(\omega_1)$ ,  $V_2(\omega_2)$  applied across a triple contact was shown to be quantized by the Euler characteristic  $\chi_F$  of the Fermi surface [70]. We note that contrary to graphene, the presence of non-trivial Euler class  $\chi$  allows for  $2|\chi|$  topologically-protected linear nodes of same chirality, which formally is a consequence of Poincare-Hopf index theorem [30]. In the Euler phases with topologically-protected underdoped linear nodes, hence with  $\chi_F = 2|\chi|$ , the nonlinear conductance  $\alpha_i(\omega_1, \omega_2)$  therefore reads [70],

$$\alpha_i(\omega_1, \omega_2) = \frac{2e^3}{\hbar^2} |\chi| \frac{1}{(\omega_1 - i0^+)(\omega_2 - i0^+)}. \quad (13)$$

We conclude by noting that unlike in the case of graphene, where nodes of opposite chiralities can be pair-annihilated, a similar attempt to mutually annihilate linear nodes in Euler phases results in merging these into a quadratic node, as long as the  $\mathcal{C}_2\mathcal{T}$  symmetry is preserved. Hence, unlike in graphene, the quantized ballistic conductance of underdoped Euler semimetals can result in the change of parity of associated  $\chi_F$ , as two nodes result in one, rather than in none [30, 37]. This observation directly reflects the circumvention of Nielsen-Ninomiya fermion doubling theorem admitted by the systems with non-trivial Euler class [37, 38]. As we predict here, this should be in principle directly observable under the triple-contact conductance measurements of Eu-

ler phases, through the characteristic parity flip of the quantized nonlinear response. Importantly, such parity-flipping through the merging, or splitting, of non-Abelian band nodes [38, 43] could be achieved by applying tensile strains under the experimental conditions applicable to real materials.

*Discussion.*— In this work, we considered anomalous bulk and wavepacket responses induced by the geometry and topology of Euler bands. We anticipate our results to be of relevance to kagome materials [71] and honeycomb multilayers [72], in the cases in which the interactions do not spontaneously break  $\mathcal{C}_2\mathcal{T}$  symmetry. It should be stressed that if  $\mathcal{T}$ -symmetry is broken as well, breaking the  $\mathcal{C}_2\mathcal{T}$  symmetry in Euler bands can induce the formation of Chern bands [73], which were experimentally and theoretically studied in a range of kagome systems [74–76]. Alternatively, breaking  $\mathcal{P}$ -symmetry, but preserving  $\mathcal{T}$ -symmetry instead, could yield second-order nonlinear Berry curvature dipole Hall responses [77] (see App. H).

While the stability of the presented unconventional transport signatures of Euler semimetals against disorder [32] and interactions naturally present in realistic materials is left for future study, we expect the geometric enhancement of the bulk responses to be a robust feature, as long as the quantization of the Euler invariant is present. Another important aspect arises from the fact that the Euler topology can be realized in a pair of fully degenerate bands over BZ, where it is equivalent within a unitary transformation to a pair of opposite Chern bands  $C = \pm\chi$  with the opposite Wilson loop windings protected by the  $\mathcal{C}_2\mathcal{T}$  symmetry [50]. In such case, no bulk Hall responses are expected, as the opposite Chern sectors ensure that the Hall responses cancel at any order in electric field. However, the fully degenerate limit over BZ remains singular and highly-tuned, i.e. the electronic structures of real materials break such model degeneracies, as known from the context of magic-angle twisted bilayer graphene (MATBG) [78], for example. As supported by the Poincare-Hopf theorem, in the non-degenerate limit [30], the Euler nodes need to remain as long as the symmetry is preserved. In such cases, any filling controlled by external voltage allows one to access the transport features underpinned by the Euler-invariant-induced singular quantum geometry, as shown in this work. As such, we expect that even minimal doping of non-degenerate Euler bands in real materials should allow accessing the invariant, as demonstrated explicitly in the previous sections.

*Conclusion.*— We unravel nonlinear transport signatures induced by the non-Abelian topologies of Euler bands and associated Riemannian quantum geometry. We obtain the manifestations of Euler topology via geodesic equations and geodesic deviations of individual wavepackets. Furthermore, we find nonlinear bulk Hall currents at second and third orders in electric field, as induced by the quantum geometry of Euler semimetals in the presence and absence of individual inversion and time-reversal symmetries. We anticipate that our results

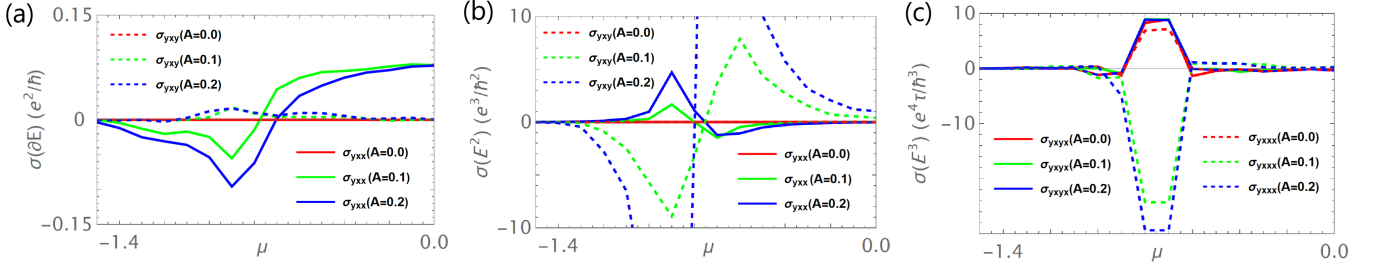


**FIG. 3.** Bulk anomalous Hall responses induced by the non-trivial Euler class associated with a topological band node. The band node appears at the chemical potential  $\mu = -0.8$  within the kagome lattice model (see App. C). We retrieve the response to the nonuniform electric fields (a), and uniform electric fields (b)–(c) at nonlinear (i.e. second/third) orders. We compute the anomalous conductivities at different chemical potentials  $\mu$  which fix the band occupations in the Euler Hamiltonian on a kagome lattice for different strengths ( $A$ ) of inversion-symmetry breaking terms. (a)–(b) The currents in response to electric field gradients  $\partial_\alpha E_\beta$  and geometric Hall currents quadratic in  $E_\alpha$  emerge when  $A \neq 0$ . (c) On the contrary, the third-order Hall response arises even when the inversion symmetry is not broken.

could serve as smoking-gun probes of exotic non-Abelian band topology in two-dimensional, e.g. kagome or honeycomb multilayer, systems.

#### ACKNOWLEDGMENTS

The authors cordially thank Adrien Bouhon, F. Nur Ünal, Giandomenico Palumbo, and Gaurav Chaudhary,

for numerous discussions on non-Abelian band topologies and quantum geometry. W.J.J. acknowledges funding from the Rod Smallwood Studentship at Trinity College, Cambridge. R.-J.S. acknowledges funding from an EPSRC ERC underwrite grant EP/X025829/1, and a Royal Society exchange grant IES/R1/221060 as well as Trinity College, Cambridge.

#### Appendix A: Derivation of the momentum-space geodesic equation

We derive the geodesic equation on introducing perturbative field-induced energy and eigenstate corrections. Here, we consider the following perturbation Hamiltonian:

$$\Delta \hat{H} = \Delta \hat{H}_E^{(1)} + \Delta \hat{H}_{\partial E}^{(2)} = e\hat{\mathbf{r}} \cdot \mathbf{E} + e\hat{\mathbf{r}} \cdot (\hat{\mathbf{r}} \cdot \nabla)\mathbf{E}, \quad (\text{A1})$$

where we assume that the electric-field gradient perturbation which arises from the nonuniformity of electric field is weaker than the electric field perturbation itself. In this work, we consider all the coupling to electric fields manifestly in length gauge. Within the perturbative expansion, we have:  $\varepsilon_{n\mathbf{k}} \rightarrow \tilde{\varepsilon}_{n\mathbf{k}} = \varepsilon_{n\mathbf{k}}^{(0)} + \varepsilon_{n\mathbf{k}}^{(1)} + \varepsilon_{n\mathbf{k}}^{(2)} + \dots$ , with  $\varepsilon_{n\mathbf{k}}^{(0)} = \varepsilon_{n\mathbf{k}}$ , the unperturbed energy, and the perturbative corrections to the eigenstates  $|\psi_{n\mathbf{k}}\rangle = e^{i\mathbf{k} \cdot \hat{\mathbf{r}}} |u_{n\mathbf{k}}\rangle$ :  $|u_{n\mathbf{k}}\rangle \rightarrow |\tilde{u}_{n\mathbf{k}}\rangle = |u_{n\mathbf{k}}^{(0)}\rangle + |u_{n\mathbf{k}}^{(1)}\rangle + |u_{n\mathbf{k}}^{(2)}\rangle + \dots$ , both of which modify the wavepacket group velocity  $\dot{\mathbf{r}}_c$ . The first-order correction to Bloch eigenstates reads,

$$|u_{n\mathbf{k}}^{(1)}\rangle = \frac{\langle \psi_{m\mathbf{k}} | \Delta \hat{H} | \psi_{n\mathbf{k}} \rangle}{\varepsilon_{n\mathbf{k}}^{(0)} - \varepsilon_{m\mathbf{k}}^{(0)}} |u_{m\mathbf{k}}^{(0)}\rangle \approx \frac{e\mathbf{E} \cdot \mathbf{A}_{nm}}{\varepsilon_{n\mathbf{k}}^{(0)} - \varepsilon_{m\mathbf{k}}^{(0)}} |u_{m\mathbf{k}}^{(0)}\rangle \equiv eE_\alpha M_{nm}^\alpha |u_{m\mathbf{k}}^{(0)}\rangle, \quad (\text{A2})$$

where  $\mathbf{A}_{nm} \equiv i \langle u_{n\mathbf{k}} | \nabla_{\mathbf{k}} u_{m\mathbf{k}} \rangle$  is the non-Abelian Berry connection, and  $M_{nm}^\alpha \equiv \frac{A_{nm}^\alpha}{\varepsilon_{n\mathbf{k}}^{(0)} - \varepsilon_{m\mathbf{k}}^{(0)}} (1 - \delta_{mn})$ .

Following the notation introduced in the main text, the wavepacket state reads

$$|\psi_n(t)\rangle = \int_{\mathbf{k}} e^{i\mathbf{k} \cdot \mathbf{r}} \left( a_n(\mathbf{k}, t) |u_{n\mathbf{k}}^{(0)}\rangle + \sum_{m \neq n} a_m(\mathbf{k}, t) |u_{m\mathbf{k}}^{(0)}\rangle \right), \quad (\text{A3})$$

with  $|a_m(\mathbf{k}, t)| \approx eE_\alpha |M_{nm}^\alpha|$ . The centre-of-mass position of the wavepacket reads  $\mathbf{r}_c(t) = \langle \psi_n(t) | \hat{\mathbf{r}} | \psi_n(t) \rangle$ , whereas the centre-of-mass momentum reads,  $\mathbf{k}_c(t) = \langle \psi_n(t) | \hat{\mathbf{p}} | \psi_n(t) \rangle$ , with momentum  $\hat{\mathbf{p}} = i\nabla_{\mathbf{r}}$ . The energy of the wavepacket reads  $\tilde{\varepsilon}_{n\mathbf{k}} = \langle \psi_n(t) | \hat{H} | \psi_n(t) \rangle$ , with  $\hat{H} = \hat{H}_0 + \Delta \hat{H}$ , and for brevity, we write  $\mathbf{k} = \mathbf{k}_c$  for the centre-of-mass momentum.

The first-order energy correction reads,

$$\varepsilon_{n\mathbf{k}}^{(1)} = \langle \psi_n(t) | \Delta H | \psi_n(t) \rangle = eE_\alpha \cdot (\mathbf{r}_c)_\alpha + e\partial_{(\alpha} E_\beta \rangle \langle \psi_n(t) | (\hat{r})_\alpha (\hat{r})_\beta | \psi_n(t) \rangle. \quad (\text{A4})$$

where we introduced an electric-field gradient  $\partial_{(\alpha} E_\beta)$  symmetrized in spatial indices  $\alpha, \beta$ . Following Ref. [59], we utilize the relation between the spread of the wavepacket and the quantum metric;  $\langle \psi_n(t) | \hat{r}_\alpha \hat{r}_\beta | \psi_n(t) \rangle \approx (\mathbf{r}_c)_\alpha (\mathbf{r}_c)_\beta + g_{\alpha\beta}^n(\mathbf{k}_c)$ . Notably, here, only the metric term  $g_{\alpha\beta}^n(\mathbf{k}_c)$  enters the group velocity for the energy correction  $\varepsilon_{n\mathbf{k}}^{(1)}$ . The second-order energy correction, consistently with the time-independent perturbation theory, reads

$$\varepsilon_{n\mathbf{k}}^{(2)} = \sum_{m \neq n} \frac{|\langle \psi_{n\mathbf{k}} | \Delta H | \psi_{m\mathbf{k}} \rangle|^2}{\varepsilon_{n\mathbf{k}}^{(0)} - \varepsilon_{m\mathbf{k}}^{(0)}} = -e^2 E_\alpha G_{\alpha\beta}^n E_\beta, \quad (\text{A5})$$

where  $G_{\alpha\beta}^n = \hbar \text{Re} \sum_{m \neq n} \frac{A_{nm}^\alpha A_{mn}^\beta}{\varepsilon_{n\mathbf{k}}^{(0)} - \varepsilon_{m\mathbf{k}}^{(0)}} = \hbar \sum_{m \neq n} \frac{g_{\alpha\beta}^{nm}}{\varepsilon_{n\mathbf{k}}^{(0)} - \varepsilon_{m\mathbf{k}}^{(0)}}$ , the weighted quantum metric defined in the main text. Here, we recognize that  $\langle \psi_{n\mathbf{k}} | \mathbf{r} | \psi_{n\mathbf{k}} \rangle = i \langle u_{m\mathbf{k}} | \nabla_{\mathbf{k}} u_{n\mathbf{k}} \rangle = A_{mn}(\mathbf{k})$  and employ the weighted quantum geometric tensor (QGT)  $\mathcal{Q}_{\alpha\beta}^n(\mathbf{k}) = \sum_m c_{mn} A_{nm}^\alpha A_{mn}^\beta$ , with weights  $c_{mn} = \frac{\hbar}{\varepsilon_{n\mathbf{k}} - \varepsilon_{m\mathbf{k}}}$ . We now combine the energy corrections and utilize the notation from the main text  $\mathcal{G}_{\alpha\beta}^n(E^2) \equiv G_{\alpha\beta}^n$ , and  $\mathcal{G}_{\alpha\beta}^n(\nabla) \equiv g_{\alpha\beta}^n$ . On differentiating with respect to the centre-of-mass momentum  $\mathbf{k}_c$ , we have,

$$\partial_{k_\gamma} \tilde{\varepsilon}_{n\mathbf{k}} \approx \partial_{k_\gamma} \varepsilon_{n\mathbf{k}} + e^2 \partial_{k_\gamma} \mathcal{G}_{\alpha\beta}^n(E^2) E_\alpha E_\beta + \frac{e}{2} \partial_{k_\gamma} \mathcal{G}^n(\nabla)_{\alpha\beta}(E^2) \partial_\alpha E_\beta. \quad (\text{A6})$$

Notably, the symmetry in electric fields picks the symmetric parts of the QGTs, i.e. the weighted quantum metrics  $\mathcal{G}_{\alpha\beta}^n(\mathbf{k}) \equiv \text{Re} \mathcal{Q}_{\alpha\beta}^n(\mathbf{k})$ . Having deduced the wavepacket energy corrections, we now deduce the wavepacket velocity satisfying a semiclassical equation of motion. Using time-dependent Schrödinger equation, and the definition of the centre-of-mass position  $\hat{\mathbf{r}}_c$ , the wavepacket velocity reads  $(\hat{\mathbf{r}}_c)_\alpha = \langle \psi_n(t) | \frac{i}{\hbar} [H, \hat{r}_\alpha] | \psi_n(t) \rangle \approx \frac{1}{\hbar} \langle \tilde{u}_{n\mathbf{k}} | \partial_{k_\alpha} H | \tilde{u}_{n\mathbf{k}} \rangle$ . Apart from the energy correction, which is symmetric in spatial indices, antisymmetric corrections associated with the perturbed Berry curvature can arise. Here, the Berry curvature enters through interband terms,

$$\left\langle u_{n\mathbf{k}}^{(0)} \left| \partial_{k_\alpha} H \right| u_{n\mathbf{k}}^{(1)} \right\rangle + \text{c.c.} = eE_\beta A_{nm}^\beta \frac{\left\langle u_{n\mathbf{k}}^{(0)} \left| \partial_{k_\alpha} H \right| u_{m\mathbf{k}}^{(0)} \right\rangle}{\varepsilon_{n\mathbf{k}}^{(0)} - \varepsilon_{m\mathbf{k}}^{(0)}} + \text{c.c.} = -ieE_\beta A_{nm}^\beta A_{mn}^\alpha + \text{c.c.} = -eE_\beta \Omega_{\beta\alpha}^n, \quad (\text{A7})$$

with Berry curvature  $\Omega_{\alpha\beta}^n = -2\text{Im} \sum_m A_{nm}^\alpha A_{mn}^\beta$ , which defines the pseudovector:  $(\boldsymbol{\Omega}_n)_\gamma = (\nabla_{\mathbf{k}} \times \mathbf{A}_{nn})_\gamma = \frac{1}{2} \epsilon_{\alpha\beta\gamma} \Omega_{\alpha\beta}^n$ . Similarly to the energies, the Berry curvature becomes perturbed at nonlinear order  $\boldsymbol{\Omega}_n \rightarrow \boldsymbol{\Omega}_n + \boldsymbol{\Omega}'_n$ , with  $\boldsymbol{\Omega}'_n \equiv \nabla_{\mathbf{k}} \times \mathbf{A}'_{nn}$ , the field-induced Berry curvature correction arising from the field-induced correction to the Berry connection  $\mathbf{A}'_{nn} = i \left\langle u_{n\mathbf{k}}^{(0)} \left| \nabla_{\mathbf{k}} u_{n\mathbf{k}}^{(1)} \right\rangle + \text{c.c.}$  [57]. On inserting  $|u_{n\mathbf{k}}^{(1)}\rangle$ :  $(\mathbf{A}'_{nn})_\alpha = G_{\alpha\beta}^n E_\beta$  [57], which in a matrix form can be written as  $\boldsymbol{\Omega}'_n = \nabla_{\mathbf{k}} \times (\underline{\underline{G}}^n \mathbf{E})$ . In particular, in an Euler Hamiltonian,  $\tilde{\boldsymbol{\Omega}}_n = \boldsymbol{\Omega}'_n$ , as  $\boldsymbol{\Omega}_n$  vanishes by  $\mathcal{C}_2\mathcal{T}$  ( $\mathcal{PT}$ ) symmetry.

On combining with the definition of the centre-of-mass velocity, we now arrive at,

$$(\hat{\mathbf{r}}_c)_\gamma = \frac{1}{\hbar} \partial_{k_\gamma} \tilde{\varepsilon}_{n\mathbf{k}} - \frac{e}{\hbar} [\mathbf{E} \times \tilde{\boldsymbol{\Omega}}_n]_\gamma = \frac{1}{\hbar} \partial_{k_\gamma} \varepsilon_{n\mathbf{k}} - \frac{e}{\hbar} [\mathbf{E} \times \tilde{\boldsymbol{\Omega}}_n]_\gamma + \frac{e^2}{\hbar^2} \partial_{k_\gamma} \mathcal{G}_{\alpha\beta}^n(E^2) E_\alpha E_\beta + \frac{e}{2\hbar} \partial_{k_\gamma} \mathcal{G}_{\alpha\beta}^n(\nabla) \partial_\alpha E_\beta, \quad (\text{A8})$$

which is the final result governing the semiclassical wavepacket equation of motion, implicitly retrieving the geodesic equation in momentum space. Namely, on replacing  $\mathbf{k}_c = -\frac{e}{\hbar} \mathbf{E}$ , we arrive at an electric field gradient-forced form of a ‘‘momentum-space geodesic equation’’ [67],

$$(\hat{\mathbf{r}}_c)_\gamma = \frac{1}{\hbar} \partial_{k_\gamma} \varepsilon_{n\mathbf{k}} - [\dot{\mathbf{k}}_c \times (\nabla_{\mathbf{k}} \times (\underline{\underline{G}}^n(E^2) \dot{\mathbf{k}}_c))]_\gamma + \partial_{k_\gamma} \mathcal{G}_{\alpha\beta}^n(E^2) (\dot{\mathbf{k}}_c)_\alpha (\dot{\mathbf{k}}_c)_\beta + \frac{e}{2\hbar} \partial_{k_\gamma} \mathcal{G}^n(\nabla)_{\alpha\beta}(E^2) \partial_\alpha E_\beta, \quad (\text{A9})$$

which completes the derivation central to this section.

## Appendix B: Derivation of the momentum-space geodesic deviation equation

Here, we derive the momentum-space geodesic deviation equation in the uniform electric fields. We furthermore show how the momentum-space Riemann curvature could be extracted from the wavepacket dynamics, on setting controllable electric field strengths.

We begin with the geodesic equation in momentum space and for the purposes of this section, set  $e = \hbar = 1$ . The simplified final result of App. A then reads,

$$(\dot{\mathbf{r}}_c)_\gamma = \partial_{k_\gamma} \tilde{\varepsilon}_{n\mathbf{k}} + \left( \partial_{k_\gamma} \mathcal{G}_{\alpha\beta}^n(E^2) - \frac{1}{2} [\partial_{k_\alpha} \mathcal{G}_{\beta\gamma}^n(E^2) + \partial_{k_\beta} \mathcal{G}_{\alpha\gamma}^n(E^2)] \right) \dot{k}_\alpha \dot{k}_\beta, \quad (\text{B1})$$

which using the definition of a Christoffel symbol from the main text reduces to,

$$(\dot{\mathbf{r}}_c)_\gamma = \partial_{k_\gamma} \tilde{\varepsilon}_{n\mathbf{k}} + \left( \frac{1}{2} \partial_{k_\gamma} \mathcal{G}_{\alpha\beta}^n(E^2) - \Gamma_{\gamma\alpha\beta}^n(E^2) \right) \dot{k}_\alpha \dot{k}_\beta. \quad (\text{B2})$$

We further utilize the definition of the weighted momentum-space Riemann tensor introduced in the main text,

$$\mathcal{R}_{\alpha\beta\gamma\delta}^n = \partial_{k_\delta} \Gamma_{\alpha\beta\gamma}^n - \partial_{k_\gamma} \Gamma_{\alpha\beta\delta}^n + \Gamma_{\mu\alpha\delta}^n \Gamma_{\beta\mu\gamma}^n - \Gamma_{\nu\beta\delta}^n \Gamma_{\alpha\nu\gamma}^n \quad (\text{B3})$$

where  $\mu$  and  $\nu$  are dummy indices. On differentiating Eq.(B2) with respect to  $k_\delta$ , we obtain

$$\partial_{k_\delta} (\dot{\mathbf{r}}_c)_\gamma = \partial_{k_\delta} \partial_{k_\gamma} \tilde{\varepsilon}_{n\mathbf{k}} + \partial_{k_\delta} \left[ \frac{1}{2} \partial_{k_\gamma} \mathcal{G}_{\alpha\beta}^n - \Gamma_{\gamma\alpha\beta}^n \right] \dot{k}_\beta \dot{k}_\alpha + \left[ \frac{1}{2} \partial_{k_\gamma} \mathcal{G}_{\alpha\beta}^n - \Gamma_{\gamma\alpha\beta}^n \right] \partial_{k_\delta} (\dot{k}_\beta \dot{k}_\alpha) \quad (\text{B4})$$

$$= \partial_{k_\delta} \partial_{k_\gamma} \tilde{\varepsilon}_{n\mathbf{k}} + \partial_{k_\delta} \left[ \frac{1}{2} \partial_{k_\gamma} \mathcal{G}_{\alpha\beta}^n - \Gamma_{\gamma\alpha\beta}^n \right] \dot{k}_\beta \dot{k}_\alpha + \left[ \frac{1}{2} \partial_{k_\gamma} \mathcal{G}_{\alpha\beta}^n - \Gamma_{\gamma\alpha\beta}^n \right] (\dot{k}_\alpha (\partial_{k_\delta} \partial_t k_\beta) + \dot{k}_\beta (\partial_{k_\delta} \partial_t k_\gamma)) \quad (\text{B5})$$

$$= \partial_{k_\delta} \partial_{k_\gamma} \tilde{\varepsilon}_{n\mathbf{k}} + \partial_{k_\delta} \left[ \frac{1}{2} \partial_{k_\gamma} \mathcal{G}_{\alpha\beta}^n - \Gamma_{\gamma\alpha\beta}^n \right] \dot{k}_\beta \dot{k}_\alpha + \left[ \frac{1}{2} \partial_{k_\gamma} \mathcal{G}_{\alpha\beta}^n - \Gamma_{\gamma\alpha\beta}^n \right] (\dot{k}_\alpha \partial_t \delta_{\delta\beta} + \dot{k}_\beta \partial_t \delta_{\delta\gamma}) \quad (\text{B6})$$

$$= \partial_{k_\delta} \partial_{k_\gamma} \tilde{\varepsilon}_{n\mathbf{k}} + \frac{1}{2} \partial_{k_\delta} \partial_{k_\gamma} \mathcal{G}_{\alpha\beta}^n \dot{k}_\beta \dot{k}_\alpha - \partial_{k_\delta} \Gamma_{\gamma\alpha\beta}^n \dot{k}_\beta \dot{k}_\alpha, \quad (\text{B7})$$

where we have used the fact that the partial derivatives commute. Antisymmetrizing with respect to  $\gamma$  and  $\delta$ , and using again the commutativity of derivatives, the first term on the right-hand-side cancels out. Using Eq. (B3) and rearranging yields

$$\frac{1}{\dot{k}_\beta \dot{k}_\alpha} \left( \partial_{k_\delta} (\dot{\mathbf{r}}_c)_\gamma - \partial_{k_\gamma} (\dot{\mathbf{r}}_c)_\delta \right) = \partial_{k_\delta} \Gamma_{\gamma\alpha\beta}^n - \partial_{k_\gamma} \Gamma_{\delta\alpha\beta}^n = \mathcal{R}_{\alpha\beta\gamma\delta}^n - \Gamma_{\beta\mu\delta} \Gamma_{\mu\gamma\alpha} + \Gamma_{\beta\nu\alpha} \Gamma_{\nu\gamma\delta}. \quad (\text{B8})$$

Substituting the values of the appropriate Christoffel symbols from Eq. (B2), this reads

$$\begin{aligned} \frac{1}{\dot{k}_\beta \dot{k}_\alpha} \left( \partial_{k_\delta} (\dot{\mathbf{r}}_c)_\gamma - \partial_{k_\gamma} (\dot{\mathbf{r}}_c)_\delta \right) &= \mathcal{R}_{\alpha\beta\gamma\delta}^n - \frac{[\dot{(\mathbf{r}}_c)_\delta - \partial_{k_\delta} \tilde{\varepsilon}_{n\mathbf{k}} - \frac{1}{2} \partial_{k_\delta} \mathcal{G}_{\beta\mu}^n] [\dot{(\mathbf{r}}_c)_\gamma - \partial_{k_\gamma} \tilde{\varepsilon}_{n\mathbf{k}} - \frac{1}{2} \partial_{k_\gamma} \mathcal{G}_{\alpha\mu}^n]}{\dot{k}_\beta \dot{k}_\mu} - \frac{[\dot{(\mathbf{r}}_c)_\gamma - \partial_{k_\gamma} \tilde{\varepsilon}_{n\mathbf{k}} - \frac{1}{2} \partial_{k_\gamma} \mathcal{G}_{\beta\nu}^n] [\dot{(\mathbf{r}}_c)_\delta - \partial_{k_\delta} \tilde{\varepsilon}_{n\mathbf{k}} - \frac{1}{2} \partial_{k_\delta} \mathcal{G}_{\nu\alpha}^n]}{\dot{k}_\nu \dot{k}_\alpha}. \end{aligned} \quad (\text{B9})$$

Clearly, the last two terms cancel (since both dummy indices  $\mu$  and  $\nu$  sum over to  $k^2$ ). This leaves us with the compact result for the deviation equation

$$\partial_{k_\delta} (\dot{\mathbf{r}}_c)_\gamma - \partial_{k_\gamma} (\dot{\mathbf{r}}_c)_\delta = \mathcal{R}_{\alpha\beta\gamma\delta}^n \dot{k}_\alpha \dot{k}_\beta. \quad (\text{B10})$$

The physical interpretation of the geodesic equation derived here is the following. The Riemannian curvature  $\mathcal{R}_{\alpha\beta\gamma\delta}^n$  determines the differences in the wavepacket evolutions governed by the center-of-mass velocities  $\dot{\mathbf{r}}_c$ , given their initial centre-of-mass momenta  $\mathbf{k}_c$ . In particular, on retrieving  $e$ ,  $\hbar$ , and inserting  $\dot{\mathbf{k}}_c = -e \frac{\mathbf{E}}{\hbar}$ , we have

$$\partial_{k_\delta} (\dot{\mathbf{r}}_c)_\gamma - \partial_{k_\gamma} (\dot{\mathbf{r}}_c)_\delta = \frac{e^2}{\hbar^2} \mathcal{R}_{\alpha\beta\gamma\delta}^n E_\alpha E_\beta, \quad (\text{B11})$$

which demonstrates that the Riemann curvature  $\mathcal{R}_{\alpha\beta\gamma\delta}^n$  can be reconstructed from wavepacket deviations, on controlling the electric field components  $\mathbf{E} = (E_x, E_y)$ .

### Appendix C: Lattice-regularized models with Euler class

Below, we provide further details on the lattice-regularized models realizing the Euler invariant. We focus on the Hamiltonians realizing the patch Euler class, as well as the net Euler class on kagome lattice. The Hamiltonian reads

$$H = \sum_i \varepsilon_i c_i^\dagger c_i - t \sum_{\langle i,j \rangle} c_i^\dagger c_j - t' \sum_{\langle\langle i,j \rangle\rangle} c_i^\dagger c_j - t'' \sum_{\langle\langle\langle i,j \rangle\rangle\rangle \in \square} c_i^\dagger c_j \quad (\text{C1})$$

where  $i, j$  run over orbitals  $A, B, C$ , where  $\varepsilon_i$  are onsite energies, and where  $t, t', t''$  are nearest neighbor ( $\langle\langle i, j \rangle\rangle$ ), next-nearest neighbor ( $\langle\langle\langle i, j \rangle\rangle\rangle$ ), next-next nearest neighbor hoppings ( $\langle\langle\langle\langle i, j \rangle\rangle\rangle\rangle$ ), and hoppings across plaquettes ( $\langle\langle\langle\langle i, j \rangle\rangle\rangle \in \odot$ ) [44, 50]. Furthermore, we add the inversion-symmetry breaking perturbations of strength  $A$ , which also breaks time-reversal symmetry, while keeping  $\mathcal{PT}$  symmetry intact. In real space, this term amounts to complex hoppings with Peierls phases  $\phi = \frac{\pi}{2}$ , equivalent to a perturbation Hamiltonian

$$H_A = -\frac{A}{2} \sum_{\langle\langle\langle i, j \rangle\rangle\rangle} e^{i\phi} c_i^\dagger c_j. \quad (\text{C2})$$

In the main text, we control the strength of the perturbation parameter  $A$  to demonstrate the emergence of second-order Hall effects, which dominate the third-order quantum-geometric Hall contributions for small, i.e. perturbative, electric field strengths  $\mathbf{E}$ . In the studied models adapted to the kagome lattice, the lower two bands realize non-trivial patch Euler class  $\chi = 1$  [43]. In this context, or the purposes of Fig. 3, we specifically set  $\varepsilon_i = 0$ ,  $t = 1$ ,  $t' = -0.2$ ,  $t'' = 0$ .

#### Appendix D: Numerical details for obtaining wavepacket trajectories

Here we provide further numerical details for obtaining the wavepacket trajectories demonstrated in Fig. 2 of the main text. The systems were initialized with a three-band gapless kagome Hamiltonian as described in App. C [43], with parameters  $\varepsilon_A = \varepsilon_B = \varepsilon_C = 0$ ,  $t = 1$ , and  $t' = -0.2$  on a hexagonal lattice with primitive reciprocal vectors  $k_1, k_2 = \pm\frac{3}{2}k_x + \frac{\sqrt{3}}{2}k_y$ . The eigenvectors of this Hamiltonian were used to calculate the multiband quantum metrics  $g_{\alpha\beta}^{mn}$  via the non-Abelian Berry connections for all ordered band pairs. The weighted metrics  $\mathcal{G}_{\alpha\beta}^{mn}$  for the nonuniform electric field and nonlinear field coupling were then found, which in turn yielded the field-induced Berry curvature corrections  $\tilde{\Omega}_n(\mathbf{E})$ . The wavepacket evolution was subsequently obtained via simultaneous numerical solution of the semiclassical equation of motion (Eq. (7) for nonuniform fields and Eq. (8) for nonlinear coupling) for position and momentum as a function of time. All the wavepackets were initialized at the origin in real space, but at several different momenta in the BZ, in order to probe the effects of proximity to the nodes at the  $\Gamma$  and  $K$  points. The numerical solver was implemented in Wolfram Mathematica 14.1 with the *Residual* method where a DAE solver was used with maximum time step size  $\Delta t = 0.1$ . The resultant numerical solutions demonstrating the anomalous Euler wavepacket propagation induced by the geodesic (App. A) and geodesic deviation equations (App. B) is shown in Fig. 2 of the main text.

#### Appendix E: Numerical momentum-space horizons

We here describe the evaluation of the momentum space horizons referred to in the main text. Correspondingly, we use the field-induced Berry curvature corrections  $\tilde{\Omega}_n(\mathbf{E})$  obtained in the aforementioned wavepacket evolution simulation (see App. A and App. D). A regular mesh of initial momenta  $\mathbf{k}_0$  in the BZ  $[(-\pi, \pi) \times (-\pi, \pi)]$  with spacing  $\Delta k = 0.3$  was subjected to the same DAE solver. Evolution into the quantum-metric singularity was tabulated for each point, in both nonuniform fields and nonlinear coupling, depending on whether the wavepacket trajectories evolved to divergent distances from the origin due to the singular geometric term, within the time interval probed. We present the tabulated result in Fig. 4. The results were verified for different spacings and electric field directions, where we obtained analogous horizons satisfying the symmetries of the kagome lattice which were explicitly broken with the external electric fields that drive the wavepacket evolution. Notably, the combined momentum-space horizons within bands  $n = 1$  and  $n = 3$  overlap with the horizons obtained in band  $n = 2$ , consistently with the band dispersion and multiband quantum geometry of two nodal subspaces realized between three bands.

#### Appendix F: Riemannian geometry of an Euler node

In the following, we fully characterize the Riemannian geometry of a non-Abelian band singularity hosting Euler class. The continuum Hamiltonian of an Euler node reads [34, 37, 79]

$$H_\chi(\mathbf{k}) = \alpha(k_+^{2|\chi|}\sigma_- + k_-^{2|\chi|}\sigma_+), \quad (\text{F1})$$

with constant  $\alpha$  fixing a band dispersion,  $k_\pm = k_x \pm ik_y$ , and  $\sigma_\pm = (\sigma_x \pm i\sigma_z)/2$ , which manifestly satisfies the  $C_2\mathcal{T}$  symmetry, allowing to write the Hamiltonian in a real gauge  $[H(\mathbf{k}) = H^*(\mathbf{k})]$ , with real eigenvectors. Real eigenvectors

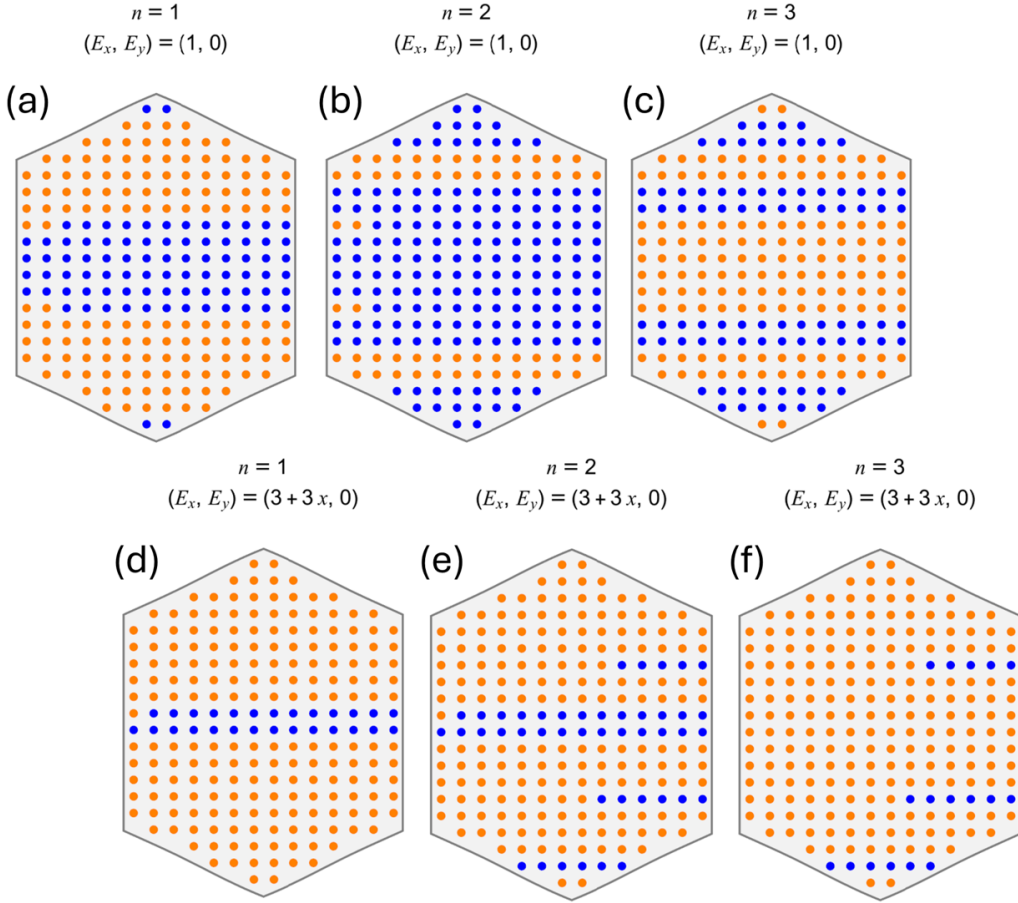


**FIG. 4.** Momentum-space horizons induced by the singular quantum metric, numerically retrieved from identifying the momenta of wavepackets falling into the band nodes. Individual points represent the initial wavevector  $\mathbf{k}_0$  of a wavepacket and blue (orange) colour represents divergent (convergent) evolution. Boundaries between regions show the horizons. **(a-c)**: Horizon plots on nonlinear quadratic coupling to a uniform electric field  $(E_x, E_y) = (1, 0)$  for the three energy bands. **(d-f)**: Horizon plots on coupling to a constant electric field gradient  $(E_x, E_y) = (3 + 3x, 0)$  for the three energy bands.

define a real vector bundle over the momentum space, which given the reality of the Bloch bundle, can be topologically characterized with the Euler characteristic class  $\chi \in \mathbb{Z}$ . As introduced in the main text, the Euler class  $\chi$  is associated with a singular non-Abelian connection  $\mathbf{A}_{12} = i\mathbf{a} = i\langle u_{1\mathbf{k}} | \nabla_{\mathbf{k}} u_{2\mathbf{k}} \rangle$ , which, as a direct consequence, induces a singular quantum metric  $g_{\alpha\beta}^{12}$ . From the eigenvectors of the Hamiltonian  $H(\mathbf{k})$ , that under the present symmetry can be chosen real, we directly evaluate the non-Abelian Berry connection and the quantum metric components [34],

$$g_{\alpha\beta}^{12} = A_{12}^\alpha A_{21}^\beta = \frac{\chi^2 k_\alpha k_\beta}{k^4} (2\delta_{\alpha\beta} - 1), \quad (\text{F2})$$

with  $k^2 \equiv k_x^2 + k_y^2$ . On differentiating in momentum-space parameters  $k_x, k_y$ , we further obtain the Christoffel symbols relevant to the nonlinear transport

$$\Gamma_{xxx}^{12} = \frac{1}{2} \partial_x g_{xx}^{12} = \frac{-2\chi^2 k_x k_y^2}{k^6}, \quad (\text{F3})$$

$$\Gamma_{yyy}^{12} = \frac{1}{2} \partial_y g_{yy}^{12} = \frac{-2\chi^2 k_x^2 k_y}{k^6}, \quad (\text{F4})$$

$$\Gamma_{yxx}^{12} = \partial_x g_{xy}^{12} - \frac{1}{2} \partial_y g_{xx}^{12} = \frac{\chi^2}{k^6} (3k_y^3 - k_x^2 k_y - k_x k_y^2 + k_x^3), \quad (\text{F5})$$

$$\Gamma_{xyy}^{12} = \partial_y g_{yx}^{12} - \frac{1}{2} \partial_x g_{yy}^{12} = \frac{\chi^2}{k^6} (3k_x^3 - k_y^2 k_x - k_y k_x^2 + k_y^3), \quad (\text{F6})$$

$$\Gamma_{xxy}^{12} = \Gamma_{xyx}^{12} = \frac{1}{2} \partial_y g_{xx}^{12} = \frac{\chi^2 (k_x^2 - k_y^2) k_y}{k^6}, \quad (\text{F7})$$

$$\Gamma_{yyx}^{12} = \Gamma_{yxy}^{12} = \frac{1}{2} \partial_x g_{yy}^{12} = \frac{\chi^2 (k_y^2 - k_x^2) k_x}{k^6}. \quad (\text{F8})$$

Finally, we compute the Riemann tensor within the continuum model, obtaining a single non-trivial component

$$\mathcal{R}_{xyxy}^{12} = \partial_x \Gamma_{xyy}^{12} - \partial_y \Gamma_{xyx}^{12} + \left( \Gamma_{xxx}^{12} \Gamma_{xyy}^{12} - \Gamma_{xxy}^{12} \Gamma_{xxy}^{12} \right) + \left( \Gamma_{xyx}^{12} \Gamma_{yyy}^{12} - \Gamma_{xyy}^{12} \Gamma_{yxy}^{12} \right), \quad (\text{F9})$$

where we use a general definition

$$\mathcal{R}_{\alpha\beta\gamma\delta}^{12} = \partial_{k_\gamma} \Gamma_{\alpha\beta\delta}^{12} - \partial_{k_\delta} \Gamma_{\alpha\beta\gamma}^{12} + \sum_e \left( \Gamma_{\alpha\mu\gamma}^{12} \Gamma_{\mu\beta\delta}^{12} - \Gamma_{\alpha\mu\beta}^{12} \Gamma_{\mu\gamma\delta}^{12} \right). \quad (\text{F10})$$

Correspondingly, we obtain

$$\mathcal{R}_{xyxy}^{12} = \frac{\chi^2 (5k_x^4 + 5k_y^4 - 38k_x^2 k_y^2)}{k^8}, \quad (\text{F11})$$

which further allows to compute the Kretschmann (scalar) invariant [55],

$$K = 6(\mathcal{R}_{xyxy}^{12})^2 = \frac{6\chi^4 (5k_x^4 + 5k_y^4 - 38k_x^2 k_y^2)^2}{k^{16}}. \quad (\text{F12})$$

Manifestly, the momentum space Kretschmann invariant diverges as  $K \sim |k|^{-8}$  at  $\mathbf{k} = 0$ , which corresponds to the quantum metric singularity at the momentum-space position of the Euler node. We demonstrate the singular nature of the momentum-space Christoffel symbols and momentum-space Riemann curvature in Fig. 5.

### Appendix G: Reconstructing the Euler invariant with electric fields

In the following, we outline how the Euler invariant can be reconstructed from the measurements of electric current responses to nonuniform electric fields and from the second-order currents in response to electric fields. We consider two reconstruction schemes from: (1) anomalous Euler wavepacket dynamics in nonlinear response to the electric fields and electric field gradients; (2) bulk anomalous (Hall) currents presented in the main text.

(1) In the case of *wavepackets*, deducing the trajectories,

$$(\mathbf{r}_c)_\gamma(t) = \int_0^t dt' (\dot{\mathbf{r}}_c)_\gamma(t') = \int_0^t dt' \left( \partial_{k_\gamma} \varepsilon_{n\mathbf{k}} + \frac{e^2}{\hbar^2} \left( \frac{1}{2} \partial_{k_\gamma} \mathcal{G}_{\alpha\beta}^n(E^2) - \Gamma_{\gamma\alpha\beta}^n(E^2) \right) E_\alpha(t') E_\beta(t') \right), \quad (\text{G1})$$

amounts to an integration of the geodesic equation derived in App. A. Therefore, adiabatic changes to the electric fields  $E_\alpha(t')$  could be used to extract the values of the derivatives:  $\nabla_{\mathbf{k}} \mathcal{G}_{\alpha\beta}^n(E^2)$ . Similarly, changing the electric field gradients adiabatically on top of the uniform electric fields present, allows to deduce the deflections of initial trajectories,

$$(\Delta \mathbf{r}_c)_\gamma(t) = \int_0^t dt' \left( \frac{e}{2\hbar} \partial_{k_\gamma} \mathcal{G}_{\alpha\beta}^n(\nabla) \partial_\alpha E_\beta(t') \right). \quad (\text{G2})$$

In Fig. 2, we precisely demonstrate the alteration of the wavepacket trajectories subject to the addition of electric field gradients. The gradient-induced deflections allow to extract the derivatives  $\partial_{k_\gamma} \mathcal{G}_{\alpha\beta}^n(\nabla)$ , hence the derivatives of the quantum metric are extracted, on an identification  $\mathcal{G}_{\alpha\beta}^n(\nabla) = g_{\alpha\beta}^n$ . To extract the metric itself, one can asymptotically continue, i.e. interpolate  $\partial_{k_\gamma} g_{\alpha\beta}^n$  to  $k \rightarrow \infty$ , where  $g_{\alpha\beta}^n = 0$ , consistently with the continuum models (see App. F). This fixes the integration constant for integrating the derivatives to obtain the metric:  $g_{\alpha\beta}^n(\mathbf{k}) = \int_\infty^{\mathbf{k}} d\mathbf{k}' \cdot \nabla_{\mathbf{k}'} g_{\alpha\beta}^n$ , where we perform a set of line integrals. An analogous procedure obtains  $\mathcal{G}_{\alpha\beta}^n(E^2) = G_{\alpha\beta}^n$ . Furthermore, on knowing the band

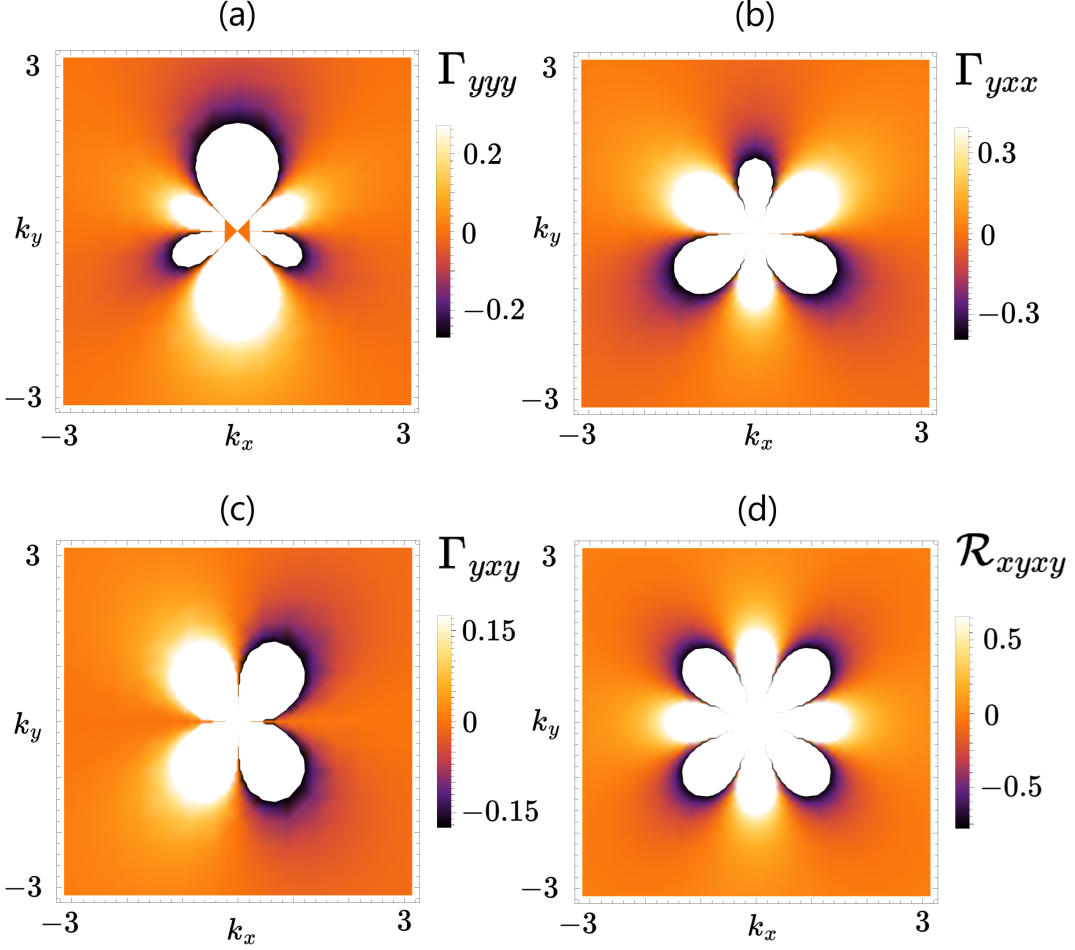


**FIG. 5.** Riemannian geometry of the continuum models with topological Euler class. We demonstrate the momentum space dependence of Christoffel symbols that enter the wavepacket geodesic equation (see App. A) and the anomalous second-order Hall responses. (a):  $\Gamma_{yyy}^{12}$ , (b):  $\Gamma_{yxx}^{12}$ , (c):  $\Gamma_{yxy}^{12}$ . (d): Momentum-space Riemann curvature  $\mathcal{R}_{xyxy}^{12}$ .  $\mathcal{R}_{xyxy}^{12}$  reflects the non-vanishing anomalous third-order conductivity due to second derivatives of quantum-metric, which were here induced by the Euler node with topological charge  $\chi = 1$ .

energies, as e.g. experimentally accessible from ARPES measurements, we evaluate the weights  $c_{mn} = \hbar/(\varepsilon_{n\mathbf{k}} - \varepsilon_{m\mathbf{k}})$ . Hence, for every  $\mathbf{k}$ -point, we arrive at a set of equations  $G_{\alpha\beta}^n = \sum_{m \neq n} c_{mn} g_{\alpha\beta}^{mn}$ , which requires to remain consistent with  $g_{\alpha\beta}^n = \sum_{m \neq n} g_{\alpha\beta}^{mn}$ . Although this protocol allows to reconstruct  $g_{\alpha\beta}^n$ , it does not provide the full multiband resolution in  $g_{\alpha\beta}^{mn}$ . However, given the singular nature of the Euler nodes, one could expect that close to the band node momentum:  $g_{\alpha\beta}^n \approx g_{\alpha\beta}^{n+1} = A_{n,n+1}^\alpha A_{n+1,n}^\beta$ , which on combining all metric coefficients  $a, b = x, y$ , allows to deduce  $A_{n,n+1}^\alpha$  up to a sign, similarly to probing the optical transition matrix elements with light [34]. As shown in Ref. [34], the Euler invariant  $\chi$  can be deduced on maximally-smooth  $\mathbb{Z}_2$  (sign) gauge fixing, which allows to reconstruct the vorticity in non-Abelian Berry connection, which defines the Euler class, as outlined in the main text.

(2) In the case of *bulk currents*, the Euler class could be inferred from the scaling of the current divergence on doping the Euler nodes. Changing  $\mu$  allows to infer the contributions to anomalous conductivities  $\sigma_{\gamma,\alpha\beta}(\nabla)$ ,  $\sigma_{\gamma,\alpha\beta}(E^2)$ ,  $\sigma_{\delta,\alpha\beta\gamma}(E^3)$ , from averages of  $\langle \partial_{k_\gamma} G_{\alpha\beta}^n \rangle_\mu$ ,  $\langle \partial_{k_\gamma} g_{\alpha\beta}^n \rangle_\mu$  at given energies  $E = \mu$ . Similarly to the wavepacket case, this allows to estimate a radial dependence of averaged  $G_{\alpha\beta}^n$ ,  $g_{\alpha\beta}^n$  from the node, which in turn allows to estimate the magnitude and scaling of  $A_{n,n+1}^\alpha$ . A radial estimate of  $A_{n,n+1}^\alpha$  allows to predict the Euler class, given the non-singular nodes (with  $\chi = 0$ ) should realize vanishing averages  $A_{n,n+1}^\alpha$ , as the vorticity in non-Abelian Berry connection is not present in such case.

## Appendix H: Derivation of the higher-order bulk Hall currents

For completeness, we derive the quantum-geometric contributions to second-order and third-order electric conductances in response to electric fields. A detailed study of third-order contributions was provided by Ref. [63]. The general approach relies on deducing the perturbative response of the free fermion eigenstates and eigenenergies, as concerning the semiclassical wavepacket dynamics (see App. A). In addition, one needs to renormalize the occupation factors of the perturbed eigenstates within the kinetic Boltzmann transport formalism:

$$\mathbf{j} = -e \int_{\mathbf{k}} \sum_n f_{n\mathbf{k}} \mathbf{v}_{n\mathbf{k}} = -e \int_{\mathbf{k}_c} \sum_n f_n(\mathbf{r}_c, \mathbf{k}_c, t) \dot{\mathbf{r}}_c. \quad (\text{H1})$$

The velocity operator matrix elements  $\mathbf{v}_{n\mathbf{k}}$  can be deduced within the approach of App. A, where we explicitly found the wavepacket velocities  $\dot{\mathbf{r}}_c$  for any band  $n$ . The distribution function  $f_n(\mathbf{r}_c, \mathbf{k}_c, t)$  can be perturbatively expanded as  $f_n = f_n^{(0)} + f_n^{(1)} + f_n^{(2)} + \dots$ , where  $f_n^{(0)} = f_{n\mathbf{k}}(\mu)$  is the equilibrium Fermi-Dirac distribution, as specified in the main text. The Boltzmann transport equation reads

$$\partial_t f_n + \dot{\mathbf{k}}_c \cdot \nabla_{\mathbf{k}} f_n + \dot{\mathbf{r}}_c \cdot \nabla_{\mathbf{r}} f_n = -\frac{f_n - f_n^{(0)}}{\tau}, \quad (\text{H2})$$

where the right-hand side corresponds to the scattering with scattering time  $\tau$ . Inserting,  $\dot{\mathbf{k}}_c = -\frac{e\mathbf{E}(\mathbf{r}_c, t)}{\hbar}$ , with  $\mathbf{E}(\mathbf{r}_c, t) = \text{Re}(\mathbf{E}e^{i\omega t})$  yields a hierarchy in frequency domain,

$$i\omega f_n^{(j+1)} + \frac{e\mathbf{E}}{\hbar} \cdot \nabla_{\mathbf{k}} f_n^{(j)} = -\frac{f_n^{(j+1)}}{\tau} \quad (\text{H3})$$

which amounts to distribution corrections in the powers of electric field strength

$$f_n^{(j)} = \left( -\frac{e}{\hbar(i\omega + 1/\tau)} \right)^j (\mathbf{E} \cdot \nabla_{\mathbf{k}})^j f_n^{(0)}. \quad (\text{H4})$$

For dc responses central to this work, we send  $\omega \rightarrow 0$ .

Equipped with the corrections in the distribution function, we now evaluate quantum-geometric contributions to third and fourth order currents. At second order, the quantum geometric term [57] on combining wavepacket velocities and perturbed distribution yields:

$$\mathbf{j}^{(2)} = -e \int_{\mathbf{k}} \sum_n f_n^{(0)} \left( -\frac{e}{\hbar} \mathbf{E} \times [\nabla_{\mathbf{k}} \times (\underline{\underline{\mathcal{G}}^n}(E^2)\mathbf{E})] \right), \quad (\text{H5})$$

which simplifies to [69],

$$\mathbf{j}_\gamma^{(2)} = -\frac{e^3}{\hbar} E_\alpha E_\beta \int_{\mathbf{k}} \sum_n f_{n\mathbf{k}}(\mu) \left( \partial_{k_\gamma} \mathcal{G}_{\alpha\beta}^n(E^2) - \frac{1}{2} [\partial_{k_\alpha} \mathcal{G}_{\beta\gamma}^n(E^2) + \partial_{k_\beta} \mathcal{G}_{\alpha\gamma}^n(E^2)] \right). \quad (\text{H6})$$

Manifestly  $\mathbf{j}^{(2)} \cdot \mathbf{E} = 0$ , showing the dissipationless (Hall) nature of the response. We calculate the corresponding second-order quantum-geometric Hall conductivity,

$$\sigma_{\gamma,\alpha\beta}^{\text{H}}(E^2) = -\frac{e^3}{\hbar} \int_{\mathbf{k}} \sum_n f_{n\mathbf{k}}(\mu) \left( \partial_{k_\gamma} \mathcal{G}_{\alpha\beta}^n(E^2) - \frac{1}{2} [\partial_{k_\alpha} \mathcal{G}_{\beta\gamma}^n(E^2) + \partial_{k_\beta} \mathcal{G}_{\alpha\gamma}^n(E^2)] \right) \quad (\text{H7})$$

for Euler Hamiltonians in the main text. Importantly, while this nonlinear Hall conductivity admits  $\mathcal{PT}$  symmetry, it requires  $\mathcal{P}$  and  $\mathcal{T}$  symmetries individually to vanish [57].

The other nonlinear Hall contribution at second order in electric fields [77],

$$\mathbf{j}^{(2)} = -e \int_{\mathbf{k}} \sum_n f_n^{(1)} \left( -\frac{e}{\hbar} [\mathbf{E} \times \boldsymbol{\Omega}_n] \right) = -\frac{e^3 \tau}{\hbar} E_\alpha E_\beta \int_{\mathbf{k}} \sum_n f_n^{(0)} \left( \partial_{k_\alpha} \Omega_{\beta\gamma}^n + \partial_{k_\beta} \Omega_{\alpha\gamma}^n \right), \quad (\text{H8})$$

associated with the Berry curvature dipole (on integrating by parts), vanishes in the Euler Hamiltonians, as  $\boldsymbol{\Omega}_n$  itself vanishes identically. On inserting  $f_n^{(2)}$ , one could analogously derive the third-order Hall Berry curvature dipole response [63], which also vanishes in the  $\mathcal{PT}$ -symmetric systems with non-trivial Euler class.

The only non-vanishing third-order Hall contribution compatible with  $\mathcal{PT}$ ,  $\mathcal{P}$ , and  $\mathcal{T}$  symmetries in centrosymmetric Euler Hamiltonians arises from the quantum metric quadrupole response, which unlike the intrinsic (i.e.  $\tau^0$  in the scattering time) quantum metric dipole Hall effect, is extrinsic, and arises from  $f_n^{(1)}$ ,

$$\mathbf{j}^{(3)} = -e \int_{\mathbf{k}} \sum_n f_n^{(1)} \left( -\frac{e}{\hbar} \left( \mathbf{E} \times [\nabla_{\mathbf{k}} \times (\underline{\underline{\mathcal{G}}}^n(E^2) \mathbf{E})] \right) \right). \quad (\text{H9})$$

On substituting for  $f_n^{(1)}$  in terms of  $f_n^{(0)}$ , and integrating by parts, we have,

$$j_\delta^{(3)} = -\frac{e^4 \tau}{3\hbar^3} \int_{\mathbf{k}} \sum_n f_n^{(0)} \left( \partial_{k_\delta} \partial_{k_{(\beta}} \mathcal{G}_{\gamma\alpha)}^n(E^2) - 3 \left( \partial_{k_{(\alpha}} \partial_{k_\beta} \mathcal{G}_{\gamma)\delta}^n(E^2) \right) \right), \quad (\text{H10})$$

which decomposes in terms of Ohmic [ $j^{(3)} \cdot \mathbf{E} \neq 0$ ] and Hall [ $j^{(3)} \cdot \mathbf{E} = 0$ ] contributions,

$$(j_\delta^{(3)})^{\text{H}} = \frac{2e^4 \tau}{3\hbar^3} \int_{\mathbf{k}} \sum_n f_n^{(0)} \left( \partial_{k_\delta} \partial_{k_{(\beta}} \mathcal{G}_{\delta\alpha)}^n(E^2) - \partial_{k_{(\alpha}} \partial_{k_\beta} \mathcal{G}_{\gamma)\delta}^n(E^2) \right), \quad (\text{H11})$$

$$(j_\delta^{(3)})^{\text{O}} = -\frac{e^4 \tau}{3\hbar^3} \int_{\mathbf{k}} \sum_n f_n^{(0)} \left( \partial_{k_{(\alpha}} \partial_{k_\beta} \mathcal{G}_{\gamma)\delta}^n(E^2) \right), \quad (\text{H12})$$

with the corresponding conductivities calculated for the Bloch Euler Hamiltonians in the main text.

Finally, at third order in electric fields, one could consider the intrinsic Hall conductivity contributions arising from Berry-connection polarizability tensor (BCT)  $T_{\alpha\beta\gamma}^n$  [60, 80]:

$$(A''_{nn})_\alpha = T_{\alpha\beta\gamma}^n E_\beta E_\gamma, \quad (\text{H13})$$

which determines a higher, second-order in electric fields, correction to the Berry curvature,  $\Omega_n'' = \nabla_{\mathbf{k}} \times \mathbf{A}_{nn}''$ . The BCT involves higher-order field-induced perturbative band corrections  $|u_{n\mathbf{k}}^{(2)}\rangle$ , and explicitly reads [63, 80]

$$T_{\alpha\beta\gamma}^n = \text{Re} \sum_{m \neq n} \left( \mathcal{U}_{\alpha\beta\gamma}^{nm} + \mathcal{U}_{\beta\alpha\gamma}^{nm} + \mathcal{U}_{\beta\gamma\alpha}^{nm} + \sum_{p \neq n, m} \mathcal{V}_{\alpha\beta\gamma}^{nmp} \right), \quad (\text{H14})$$

with two-band  $\mathcal{U}_{\alpha\beta\gamma}^{nm}$ , and three-band  $\mathcal{V}_{\alpha\beta\gamma}^{nmp}$  contributions explicitly given by the non-Abelian Berry connection contributions (see also App. A) [63, 80],

$$\mathcal{U}_{\alpha\beta\gamma}^{nm} = M_{nm}^\alpha (A_{nn}^\beta - A_{mm}^\alpha - i\partial_{k_\beta}) M_{mn}^\gamma, \quad (\text{H15})$$

$$\mathcal{V}_{\alpha\beta\gamma}^{nmp} = (2M_{nm}^\alpha A_{mp}^\beta + M_{nm}^\beta A_{mp}^\alpha) M_{pn}^\gamma. \quad (\text{H16})$$

The BCT yields intrinsic third-order currents,

$$\mathbf{j}^{(3)} = -e \int_{\mathbf{k}} \sum_n f_n^{(0)} \left( -\frac{e}{\hbar} [\mathbf{E} \times \boldsymbol{\Omega}_n''] \right), \quad (\text{H17})$$

which componentwise can be expressed as [80],

$$j_\delta^{(3)} = \frac{e^4}{\hbar} E_\alpha E_\beta E_\gamma \int_{\mathbf{k}} \sum_n f_n^{(0)} \left( \partial_{k_\beta} T_{\delta\gamma\alpha}^n - \partial_{k_\delta} T_{\beta\gamma\alpha}^n \right). \quad (\text{H18})$$

However, such intrinsic contributions are vanishing under the considered combination of  $\mathcal{PT}$ ,  $\mathcal{P}$ , and  $\mathcal{T}$  symmetries [63]. In the non-centrosymmetric case, we expect these contributions to be dominated by the second-order quantum-metric dipole Hall effect, as long as the electric fields  $\mathbf{E}$  remain moderate, and the scattering time is sufficiently long, i.e.  $\frac{|e\mathbf{E}a|}{\hbar} < \frac{1}{\tau}$ , where the lattice constant  $a$  physically determines the electric potential differences across the individual unit cells of the system.

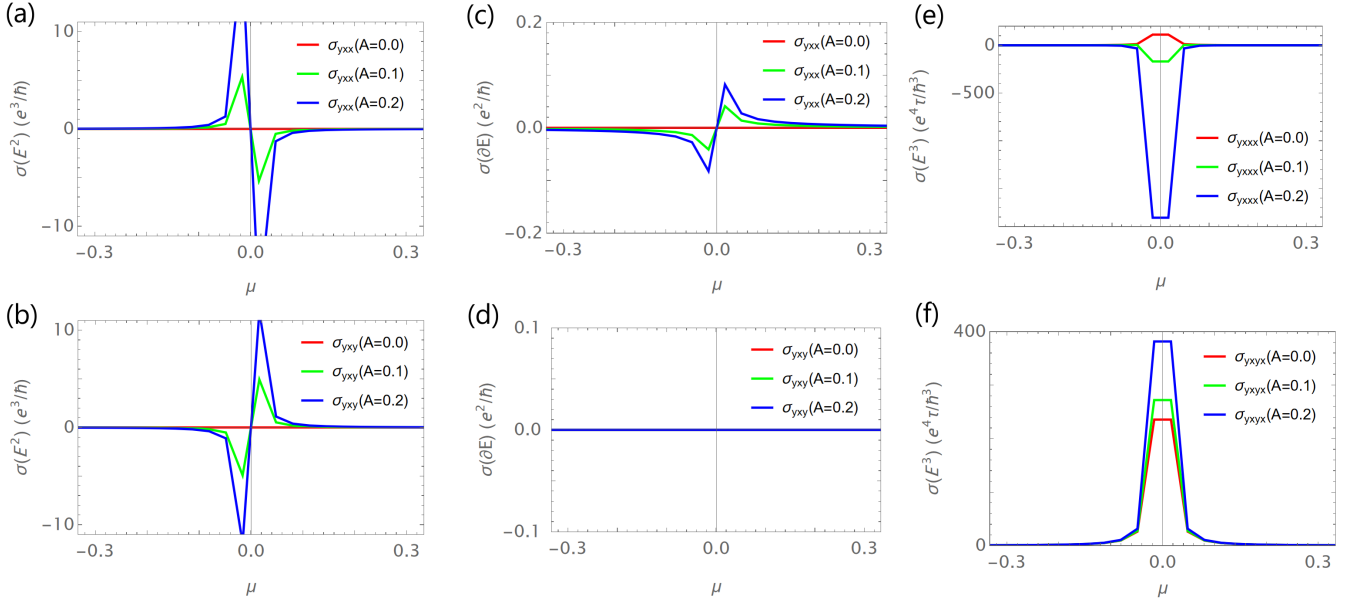


**FIG. 6.** Anomalous currents in continuum models with topological Euler class, as a function of chemical potential  $\mu$  and inversion-symmetry breaking perturbations of strength  $A$ . For analogous components of conductivity tensors within the lattice-regularized models, see Fig. 3 in the main text. **(a-b)**: Conductivities yielding geometric currents in responses to electric field gradients. **(c-d)**: Quantum-metric dipole-induced second-order Hall conductivities in responses to electric fields. **(e-f)**: Quantum-metric quadrupole-induced third-order Hall conductivities in responses to electric fields. The third-order geometric Hall response is extrinsic and directly proportional to the scattering time  $\tau$ .

### Appendix I: Bulk nonlinear currents from continuum models

Below, we demonstrate how the bulk nonlinear quantum-metric Hall responses can be directly retrieved from effective continuum models. These findings support the results obtained numerically in the lattice-regularized models hosting patch Euler class topology (App. C). As detailed in App. F, we utilize Christoffel symbols and Riemannian curvature, which we include within the response functions of the corresponding conductivities. To model the inversion-symmetry breaking perturbation (see App. C), we modify the original continuum Hamiltonian characterized in App. F with a perturbation  $H_A = Ak_x \mathbf{1}_2$ , i.e. the combined Hamiltonian reads,

$$H(\mathbf{k}) = \alpha(k_+^{2|\chi|} \sigma_- + k_-^{2|\chi|} \sigma_+) + Ak_x \mathbf{1}_2, \quad (\text{I1})$$

from which we deduce all the nonlinear responses studied in the main text. Correspondingly, we include the continuum model conductivities in Fig. 6. Having accounted for the geometric contributions of the third (trivial) band, these results remain in a good qualitative overlap with the anomalous conductance scalings between the Euler band subspace in the lattice-regularized Euler Hamiltonians (App. C) that were shown in Fig. 3.

- 
- [1] X.-L. Qi and S.-C. Zhang, Topological insulators and superconductors, *Rev. Mod. Phys.* **83**, 1057 (2011).
  - [2] M. Z. Hasan and C. L. Kane, Colloquium: Topological Insulators, *Rev. Mod. Phys.* **82**, 3045 (2010).
  - [3] N. P. Armitage, E. J. Mele, and A. Vishwanath, Weyl and Dirac semimetals in three-dimensional solids, *Rev. Mod. Phys.* **90**, 015001 (2018).
  - [4] F. D. M. Haldane, Model for a quantum Hall effect without Landau levels: Condensed-matter realization of the "parity anomaly", *Phys. Rev. Lett.* **61**, 2015 (1988).
  - [5] E. Fradkin, E. Dagotto, and D. Boyanovsky, Physical realization of the parity anomaly in condensed matter physics, *Phys. Rev. Lett.* **57**, 2967 (1986).
  - [6] M. M. Otrokov, I. I. Klimovskikh, H. Bentmann, D. Estyunin, A. Zeugner, Z. S. Aliev, S. Gaß, A. U. B. Wolter, A. V. Koroleva, A. M. Shikin, M. Blanco-Rey, M. Hoffmann, I. P. Rusinov, A. Y. Vyazovskaya, S. V. Ereemeev, Y. M. Koroteev, V. M. Kuznetsov, F. Freyse, J. Sánchez-Barriga, I. R. Amiraslanov, M. B. Babanly, N. T. Mamedov, N. A. Abdullayev, V. N. Zverev, A. Al-

- fonsov, V. Kataev, B. Büchner, E. F. Schwier, S. Kumar, A. Kimura, L. Petaccia, G. Di Santo, R. C. Vidal, S. Schatz, K. Kißner, M. Ünzelmann, C. H. Min, S. Moser, T. R. F. Peixoto, F. Reinert, A. Ernst, P. M. Echenique, A. Isaeva, and E. V. Chulkov, Prediction and observation of an antiferromagnetic topological insulator, *Nature* **576**, 416 (2019).
- [7] N. H. Jo, L.-L. Wang, R.-J. Slager, J. Yan, Y. Wu, K. Lee, B. Schruk, A. Vishwanath, and A. Kaminski, Intrinsic axion insulating behavior in antiferromagnetic  $\text{mnbi}_6\text{te}_{10}$ , *Phys. Rev. B* **102**, 045130 (2020).
- [8] X.-L. Qi, T. L. Hughes, and S.-C. Zhang, Topological field theory of time-reversal invariant insulators, *Phys. Rev. B* **78**, 195424 (2008).
- [9] H. Zhang, C.-X. Liu, X.-L. Qi, X. Dai, Z. Fang, and S.-C. Zhang, Topological insulators in  $\text{Bi}_2\text{Se}_3$ ,  $\text{Bi}_2\text{Te}_3$  and  $\text{Sb}_2\text{Te}_3$  with a single Dirac cone on the surface, *Nature Physics* **5**, 438 (2009).
- [10] D. E. Kharzeev, The chiral magnetic effect and anomaly-induced transport, *Progress in Particle and Nuclear Physics* **75**, 133–151 (2014).
- [11] S. A. Parameswaran, T. Grover, D. A. Abanin, D. A. Pesin, and A. Vishwanath, Probing the chiral anomaly with nonlocal transport in three-dimensional topological semimetals, *Phys. Rev. X* **4**, 031035 (2014).
- [12] J. Behrends, A. G. Grushin, T. Ojanen, and J. H. Bardarson, Visualizing the chiral anomaly in Dirac and Weyl semimetals with photoemission spectroscopy, *Physical Review B* **93**, 10.1103/physrevb.93.075114 (2016).
- [13] M. M. Vazifeh and M. Franz, Electromagnetic response of Weyl semimetals, *Phys. Rev. Lett.* **111**, 027201 (2013).
- [14] A. Cortijo, Y. Ferreirós, K. Landsteiner, and M. A. H. Vozmediano, Elastic gauge fields in Weyl semimetals, *Phys. Rev. Lett.* **115**, 177202 (2015).
- [15] J. Gooth, A. C. Niemann, T. Meng, A. G. Grushin, K. Landsteiner, B. Gotsmann, F. Menges, M. Schmidt, C. Shekhar, V. Süß, R. Hühne, B. Rellinghaus, C. Felser, B. Yan, and K. Nielsch, Experimental signatures of the mixed axial-gravitational anomaly in the Weyl semimetal  $\text{nbp}$ , *Nature* **547**, 324 (2017).
- [16] R.-J. Slager, The translational side of topological band insulators, *J. Phys. Chem. Solids* **128**, 24 (2019), spin-Orbit Coupled Materials.
- [17] Y. Ran, Y. Zhang, and A. Vishwanath, One-dimensional topologically protected modes in topological insulators with lattice dislocations., *Nat. Phys.* **5**, 298 (2009).
- [18] O. Parrikar, T. L. Hughes, and R. G. Leigh, Torsion, parity-odd response, and anomalies in topological states, *Physical Review D* **90**, 10.1103/physrevd.90.105004 (2014).
- [19] Y. Ferreiros, Y. Kedem, E. J. Bergholtz, and J. H. Bardarson, Mixed axial-torsional anomaly in Weyl semimetals, *Phys. Rev. Lett.* **122**, 056601 (2019).
- [20] J. Nissinen, Emergent spacetime and gravitational niehyan anomaly in chiral  $p+ip$  Weyl superfluids and superconductors, *Phys. Rev. Lett.* **124**, 117002 (2020).
- [21] J. Nissinen, Emergent geometry, torsion and anomalies in non-relativistic topological matter, *Journal of Physics: Conference Series* **2531**, 012002 (2023).
- [22] M. Stone, Gravitational anomalies and thermal Hall effect in topological insulators, *Phys. Rev. B* **85**, 184503 (2012).
- [23] J. Nissinen and G. E. Volovik, Elasticity tetrads, mixed axial-gravitational anomalies, and (3+1)-d quantum Hall effect, *Phys. Rev. Res.* **1**, 023007 (2019).
- [24] H. C. Po, A. Vishwanath, and H. Watanabe, Symmetry-based indicators of band topology in the 230 space groups, *Nat. Commun.* **8**, 50 (2017).
- [25] R.-J. Slager, A. Mesaros, V. Juričić, and J. Zaanen, The space group classification of topological band-insulators, *Nat. Phys.* **9**, 98 (2013).
- [26] J. Kruthoff, J. de Boer, J. van Wezel, C. L. Kane, and R.-J. Slager, Topological classification of crystalline insulators through band structure combinatorics, *Phys. Rev. X* **7**, 041069 (2017).
- [27] B. Bradlyn, L. Elcoro, J. Cano, M. G. Vergniory, Z. Wang, C. Felser, M. I. Aroyo, and B. A. Bernevig, Topological quantum chemistry, *Nature* **547**, 298 (2017).
- [28] K. Shiozaki and M. Sato, Topology of crystalline insulators and superconductors, *Phys. Rev. B* **90**, 165114 (2014).
- [29] C.-K. Chiu, J. C. Y. Teo, A. P. Schnyder, and S. Ryu, Classification of topological quantum matter with symmetries, *Rev. Mod. Phys.* **88**, 035005 (2016).
- [30] A. Bouhon, T. Bzdusek, and R.-J. Slager, Geometric approach to fragile topology beyond symmetry indicators, *Phys. Rev. B* **102**, 115135 (2020).
- [31] Z. Davoyan, W. J. Jankowski, A. Bouhon, and R.-J. Slager, Three-dimensional  $\mathcal{PT}$ -symmetric topological phases with a Pontryagin index, *Phys. Rev. B* **109**, 165125 (2024).
- [32] W. J. Jankowski, M. Noormandipour, A. Bouhon, and R.-J. Slager, Disorder-induced topological quantum phase transitions in multigap Euler semimetals, *Phys. Rev. B* **110**, 064202 (2024).
- [33] W. J. Jankowski, A. S. Morris, Z. Davoyan, A. Bouhon, F. N. Ünal, and R.-J. Slager, Non-Abelian Hopf-Euler insulators, *Phys. Rev. B* **110**, 075135 (2024).
- [34] W. J. Jankowski, A. S. Morris, A. Bouhon, F. N. Ünal, and R.-J. Slager, [Optical manifestations of topological Euler class in electronic materials](#) (2023), [arXiv:2311.07545 \[cond-mat.mes-hall\]](#).
- [35] W. J. Jankowski and R.-J. Slager, Quantized integrated shift effect in multigap topological phases, *Phys. Rev. Lett.* **133**, 186601 (2024).
- [36] A. Bouhon, A. M. Black-Schaffer, and R.-J. Slager, Wilson loop approach to fragile topology of split elementary band representations and topological crystalline insulators with time-reversal symmetry, *Phys. Rev. B* **100**, 195135 (2019).
- [37] J. Ahn, S. Park, and B.-J. Yang, Failure of Nielsen-Ninomiya Theorem and Fragile Topology in Two-Dimensional Systems with Space-Time Inversion Symmetry: Application to Twisted Bilayer Graphene at Magic Angle, *Phys. Rev. X* **9**, 021013 (2019).
- [38] A. Bouhon, Q. Wu, R.-J. Slager, H. Weng, O. V. Yazyev, and T. Bzdusek, Non-Abelian reciprocal braiding of Weyl points and its manifestation in  $\text{ZrTe}$ , *Nature Physics* **16**, 1137 (2020).
- [39] Q. Wu, A. A. Soluyanov, and T. Bzdusek, Non-Abelian band topology in noninteracting metals, *Science* **365**, 1273 (2019).
- [40] F. N. Ünal, A. Bouhon, and R.-J. Slager, Topological Euler class as a dynamical observable in optical lattices, *Phys. Rev. Lett.* **125**, 053601 (2020).
- [41] W. Zhao, Y.-B. Yang, Y. Jiang, Z. Mao, W. Guo, L. Qiu, G. Wang, L. Yao, L. He, Z. Zhou, Y. Xu, and

- L. Duan, Quantum simulation for topological Euler insulators, *Communications Physics* **5**, 223 (2022).
- [42] O. Breach, R.-J. Slager, and F. N. Ünal, Interferometry of non-Abelian band singularities and Euler class topology, *Phys. Rev. Lett.* **133**, 093404 (2024).
- [43] B. Jiang, A. Bouhon, Z.-K. Lin, X. Zhou, B. Hou, F. Li, R.-J. Slager, and J.-H. Jiang, Experimental observation of non-Abelian topological acoustic semimetals and their phase transitions, *Nature Physics* **17**, 1239–1246 (2021).
- [44] B. Jiang, A. Bouhon, S.-Q. Wu, Z.-L. Kong, Z.-K. Lin, R.-J. Slager, and J.-H. Jiang, Observation of an acoustic topological Euler insulator with meronic waves, *Science Bulletin* **69**, 1653 (2024).
- [45] B. Peng, A. Bouhon, B. Monserrat, and R.-J. Slager, Phonons as a platform for non-Abelian braiding and its manifestation in layered silicates, *Nature Communications* **13**, 423 (2022).
- [46] B. Peng, A. Bouhon, R.-J. Slager, and B. Monserrat, Multigap topology and non-Abelian braiding of phonons from first principles, *Phys. Rev. B* **105**, 085115 (2022).
- [47] R.-J. Slager, A. Bouhon, and F. N. Ünal, Non-Abelian Floquet braiding and anomalous Dirac string phase in periodically driven systems, *Nature Communications* **15**, 1144 (2024).
- [48] V. Könye, A. Bouhon, I. C. Fulga, R.-J. Slager, J. van den Brink, and J. I. Facio, Chirality flip of Weyl nodes and its manifestation in strained  $\text{mote}_2$ , *Phys. Rev. Res.* **3**, L042017 (2021).
- [49] S. H. Lee, Y. Qian, and B.-J. Yang, Euler band topology in spin-orbit coupled magnetic systems (2024), arXiv:2404.16383 [cond-mat.mes-hall].
- [50] T. B. Wahl, W. J. Jankowski, A. Bouhon, G. Chaudhary, and R.-J. Slager, Exact projected entangled pair ground states with topological Euler invariant (2024), arXiv:2407.12902 [quant-ph].
- [51] J. Provost and G. Vallee, Riemannian structure on manifolds of quantum states, *Communications in Mathematical Physics* **76**, 289 (1980).
- [52] J. Ahn, G.-Y. Guo, and N. Nagaosa, Low-frequency divergence and quantum geometry of the bulk photovoltaic effect in topological semimetals, *Phys. Rev. X* **10**, 041041 (2020).
- [53] J. Ahn, G.-Y. Guo, N. Nagaosa, and A. Vishwanath, Riemannian geometry of resonant optical responses, *Nature Physics* **18**, 290–295 (2021).
- [54] A. Bouhon, A. Timmel, and R.-J. Slager, Quantum geometry beyond projective single bands (2023), arXiv:2303.02180 [cond-mat.mes-hall].
- [55] E. Kretschmann, Über die prinzipielle Bestimmbarkeit der berechtigten Bezugssysteme beliebiger Relativitätstheorien (i), (ii), *Annalen der Physik* **48** (1915).
- [56] B. M. Fregoso, R. A. Muniz, and J. E. Sipe, Jerk current: A novel bulk photovoltaic effect, *Phys. Rev. Lett.* **121**, 176604 (2018).
- [57] Y. Gao, S. A. Yang, and Q. Niu, Field induced positional shift of Bloch electrons and its dynamical implications, *Phys. Rev. Lett.* **112**, 166601 (2014).
- [58] A. Gao, Y.-F. Liu, J.-X. Qiu, B. Ghosh, T. V. Trevisan, Y. Onishi, C. Hu, T. Qian, H.-J. Tien, S.-W. Chen, M. Huang, D. Bérubé, H. Li, C. Tzschaschel, T. Dinh, Z. Sun, S.-C. Ho, S.-W. Lien, B. Singh, K. Watanabe, T. Taniguchi, D. C. Bell, H. Lin, T.-R. Chang, C. R. Du, A. Bansil, L. Fu, N. Ni, P. P. Orth, Q. Ma, and S.-Y. Xu, Quantum metric nonlinear Hall effect in a topological antiferromagnetic heterostructure, *Science* **381**, 181–186 (2023).
- [59] M. F. Lapa and T. L. Hughes, Semiclassical wave packet dynamics in nonuniform electric fields, *Phys. Rev. B* **99**, 121111 (2019).
- [60] S. Lai, H. Liu, Z. Zhang, J. Zhao, X. Feng, N. Wang, C. Tang, Y. Liu, K. S. Novoselov, S. A. Yang, and W.-b. Gao, Third-order nonlinear Hall effect induced by the Berry-connection polarizability tensor, *Nature Nanotechnology* **16**, 869 (2021).
- [61] J. Mi, J. Li, M. Li, S. Xu, S. Yu, Z. Li, X. Fan, H. Zhu, Q. Tao, L. Li, and Z. Xu, Third order nonlinear transport properties in topological chiral antiferromagnetic semimetal  $\text{CoNb}_3\text{S}_6$  (2023), arXiv:2312.05824 [cond-mat.mtrl-sci].
- [62] Y. Gao, Z.-Q. Zhang, and K.-H. Ding, Third-order nonlinear Hall effect in two-dimensional Dirac systems, *New Journal of Physics* **25**, 053013 (2023).
- [63] D. Mandal, S. Sarkar, K. Das, and A. Agarwal, Quantum geometry induced third order nonlinear transport responses (2024), arXiv:2310.19092 [cond-mat.mes-hall].
- [64] H. Li, C. Zhang, C. Zhou, C. Ma, X. Lei, Z. Jin, H. He, B. Li, K. T. Law, and J. Wang, Quantum geometry quadrupole-induced third-order nonlinear transport in antiferromagnetic topological insulator  $\text{MnBi}_2\text{Te}_4$ , *Nature Communications* **15**, 7779 (2024).
- [65] Óscar Pozo Ocaña and I. Souza, Multipole theory of optical spatial dispersion in crystals, *SciPost Phys.* **14**, 118 (2023).
- [66] Y. Gao, Semiclassical dynamics and nonlinear charge current, *Frontiers of Physics* **14**, 33404 (2019).
- [67] T. B. Smith, L. Pullasserri, and A. Srivastava, Momentum-space gravity from the quantum geometry and entropy of Bloch electrons, *Phys. Rev. Res.* **4**, 013217 (2022).
- [68] Y. Gao and D. Xiao, Nonreciprocal directional dichroism induced by the quantum metric dipole, *Physical Review Letters* **122**, 10.1103/physrevlett.122.227402 (2019).
- [69] D. Kaplan, T. Holder, and B. Yan, Unification of nonlinear anomalous Hall effect and nonreciprocal magnetoresistance in metals by the quantum geometry, *Phys. Rev. Lett.* **132**, 026301 (2024).
- [70] C. Kane, Quantized nonlinear conductance in ballistic metals, *Physical Review Letters* **128**, 10.1103/physrevlett.128.076801 (2022).
- [71] M. Kang, S. Kim, Y. Qian, P. M. Neves, L. Ye, J. Jung, D. Puntel, F. Mazzola, S. Fang, C. Jozwiak, A. Bostwick, E. Rotenberg, J. Fuji, I. Vobornik, J.-H. Park, J. G. Checkelsky, B.-J. Yang, and R. Comin, Measurements of the quantum geometric tensor in solids, *Nature Physics* **10.1038/s41567-024-02678-8** (2024).
- [72] C. Mondal, R. Ghadimi, and B.-J. Yang, Non-Abelian charge conversion in bilayer binary honeycomb lattice systems (2024), arXiv:2411.06724 [cond-mat.mes-hall].
- [73] A. Bouhon and R.-J. Slager, Multi-gap topological conversion of Euler class via band-node braiding: minimal models,  $PT$ -linked nodal rings, and chiral heirs (2022), arXiv:2203.16741 [cond-mat.mes-hall].
- [74] K. Sun, Z. Gu, H. Katsura, and S. Das Sarma, Nearly flatbands with nontrivial topology, *Phys. Rev. Lett.* **106**, 236803 (2011).
- [75] G. Xu, B. Lian, and S.-C. Zhang, Intrinsic quantum

- anomalous Hall effect in the kagome lattice  $\text{Cs}_2\text{limn}_3\text{f}_{12}$ , [Phys. Rev. Lett. \*\*115\*\*, 186802 \(2015\)](#).
- [76] C. Guo, C. Putzke, S. Konyzheva, X. Huang, M. Gutierrez-Amigo, I. Errea, D. Chen, M. G. Vergniory, C. Felser, M. H. Fischer, T. Neupert, and P. J. W. Moll, Switchable chiral transport in charge-ordered kagome metal  $\text{CsV}_3\text{Sb}_5$ , [Nature \*\*611\*\*, 461–466 \(2022\)](#).
- [77] I. Sodemann and L. Fu, Quantum nonlinear Hall effect induced by Berry curvature dipole in time-reversal invariant materials, [Phys. Rev. Lett. \*\*115\*\*, 216806 \(2015\)](#).
- [78] H. C. Po, L. Zou, T. Senthil, and A. Vishwanath, Faithful tight-binding models and fragile topology of magic-angle bilayer graphene, [Phys. Rev. B \*\*99\*\*, 195455 \(2019\)](#).
- [79] A. S. Morris, A. Bouhon, and R.-J. Slager, Andreev reflection in Euler materials, [New Journal of Physics \*\*26\*\*, 023014 \(2024\)](#).
- [80] H. Liu, J. Zhao, Y.-X. Huang, X. Feng, C. Xiao, W. Wu, S. Lai, W.-b. Gao, and S. A. Yang, Berry connection polarizability tensor and third-order Hall effect, [Phys. Rev. B \*\*105\*\*, 045118 \(2022\)](#).